AUSTRALIAN JOURNAL OF EARTH SCIENCES
https://doi.org/10.1080/08120099.2026.2701983

OPEN ACCESS Check for updates

Evidence of glacial processes within the Lefroy Drainage System, Western Australia

L. Lynham[a], E. Knutsen[a,b], G. Smith[c] and R. Vaucher[a]

[a]College of Science and Engineering, James Cook University, Townsville, QLD, Australia; [b]Queensland Museum Tropics, Townsville, QLD, Australia; [c]School of Earth and Planetary Sciences, Curtin University, Perth, WA, Australia

ABSTRACT

Large-scale drainage systems traversing the Yilgarn Craton, Western Australia, have a long-debated mechanism of origin. In the northern parts of the Yilgarn Craton, direct evidence exists for their creation and fill by glacial processes (bed rock striations, polished pavements, infill of drainages by tillite), although similar evidence has not been recognised in the southern Lefroy Drainage System. This paper presents the first detailed evidence for glacially influenced sediments including pebbly diamictite, with preserved features suggesting glacial origin within the Lefroy Drainage System. This is based on data collected from field localities east of Lake Lefroy and describes the geological and paleoenvironmental history of these outcrops. Additionally, subsurface data are utilised to describe glacial morphologies from Lefroy Drainage System. These data support regional correlations of this scour and fill to other drainages across the Yilgarn Craton.

KEY POINTS

1. Glacigene sedimentary rocks associated with melt-out of debris-rich stagnant ice are described from the middle–lower reaches of the Lefroy Drainage System.
2. Using a depth-to-basement model, it is shown that the Lefroy Paleovalley exhibits clear glacial morphology of an asymmetrical U shape.
3. The evidence suggests that the Lefroy Drainage System has its initial scour in glacial processes matching established consensus for other parallel drainage systems on the Yilgarn Craton.

ARTICLE HISTORY
Received 26 February 2026
Accepted 6 July 2026

KEYWORDS
Glacial sedimentation; Late Paleozoic Ice Age (LPIA); tillite; Yilgarn Craton; Gondwana; paleodrainage; geomorphology; glacial scour

Introduction

The Late Paleozoic Ice Age (LPIA) was a series of glaciations across the Gondwanan supercontinent lasting *ca* 72 million years from 328 to 254 Ma (Fielding *et al*., 2023). The LPIA is considered to have begun during the Tournaisian (Carboniferous) in western Gondwana (modern western Argentina) (Caputo *et al*., 2008; Fielding *et al*., 2023; Pérez Loinaze *et al*., 2011) and ended in eastern Gondwana (modern eastern Australia) in the earliest Wuchiapingian (Permian) (Fielding *et al*., 2008, 2023).

In eastern Australia, the LPIA is recorded by eight, non-overlapping glacial intervals, namely: C1–C4 in the Carboniferous and P1–P4 during the Permian, which can be correlated across Gondwana (Fielding *et al*., 2008, 2023; Isbell *et al*., 2003, 2012). These intervals and their Gondwana-wide correlatives are represented by stratigraphic successions that represent ice centres that appeared diachronously across Gondwana as the supercontinent drifted towards the South Pole (Isbell *et al*., 2012).

Western Australia records extensive, but non-continuous glacigene deposition, mostly from the P1 stage (299–290 Ma) of the LPIA (*e.g.* Backhouse & Mory, 2020; Dillinger *et al*., 2022; Eyles *et al*., 2003; Fielding *et al*., 2023; Mory *et al*., 2008) with some additional evidence of P3 deglaciation (Eyles *et al*., 2002; Isbell *et al*., 2012). During the LPIA, ice cover may have been continuous across Gondwana, with either one large icesheet originating in Antarctica (*e.g.* Hyde *et al*., 1999; Scotese & Barrett, 1990; Veevers, 1994; Ziegler *et al*., 1997) or from several ice centres across the landmass (*e.g.* Crowell & Frakes, 1971; Fielding *et al*., 2008, 2023; Isbell, 2010; Isbell *et al*., 2003, 2012; Mory *et al*., 2008). Evidence for glacigene rocks from the LPIA of the Yilgarn Craton (Figure 1a), Western Australia, is restricted to isolated outcrops inferred to be the lower Permian (Sakmarian) Paterson Formation, and subsurface occurrences intersected during regional exploration programs (Collins, 2013; Eyles & de Broekert, 2001; Pickard, 2025; Salama *et al*., 2021, 2022; Salama & Anand, 2017).

The Yilgarn Craton overall exhibits very low topographic relief and is commonly described as peneplanated. However, extensive buried drainage networks, which are represented at the surface by linear chains of salt lakes (Figure 1b), are preserved in the subsurface. The low relief of the Yilgarn Craton and the preservation of these drainages have been attributed

CONTACT L. Lynham Leah.lynham@my.jcu.edu.au College of Science and Engineering, James Cook University, Townsville, QLD 4811, Australia
Supplemental data for this article can be accessed online at https://doi.org/10.1080/08120099.2026.2701983.
Editorial handling: Anita Andrew

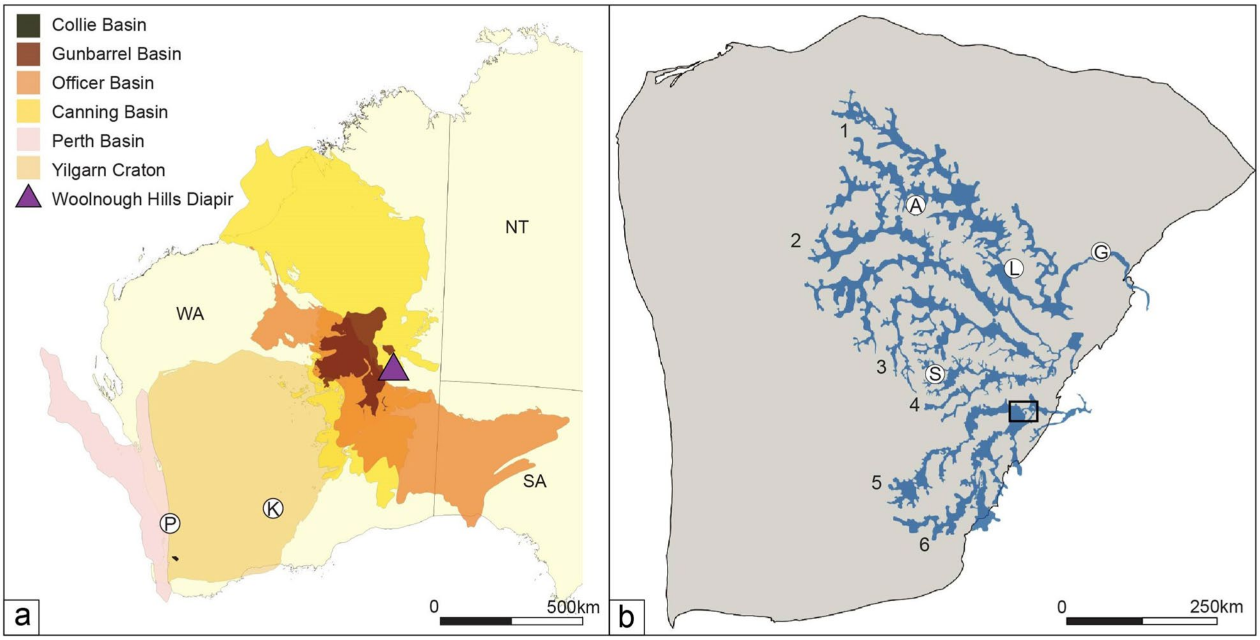

Figure 1. (a) Map of central and western Australian geological basins and cratons discussed in this text. K, Kambalda; P, Perth. (b) Drainage systems are marked by numbers: 1, Carey; 2, Raeside; 3, Rebecca; 4, Roe; 5, Lefroy; 6, Cowan. Reported buried glacial drainage infill discussed in this paper: A, Agnew; G, Gruyere; L, Laverton; S, Sand King. Black box expanded in Figure 2.

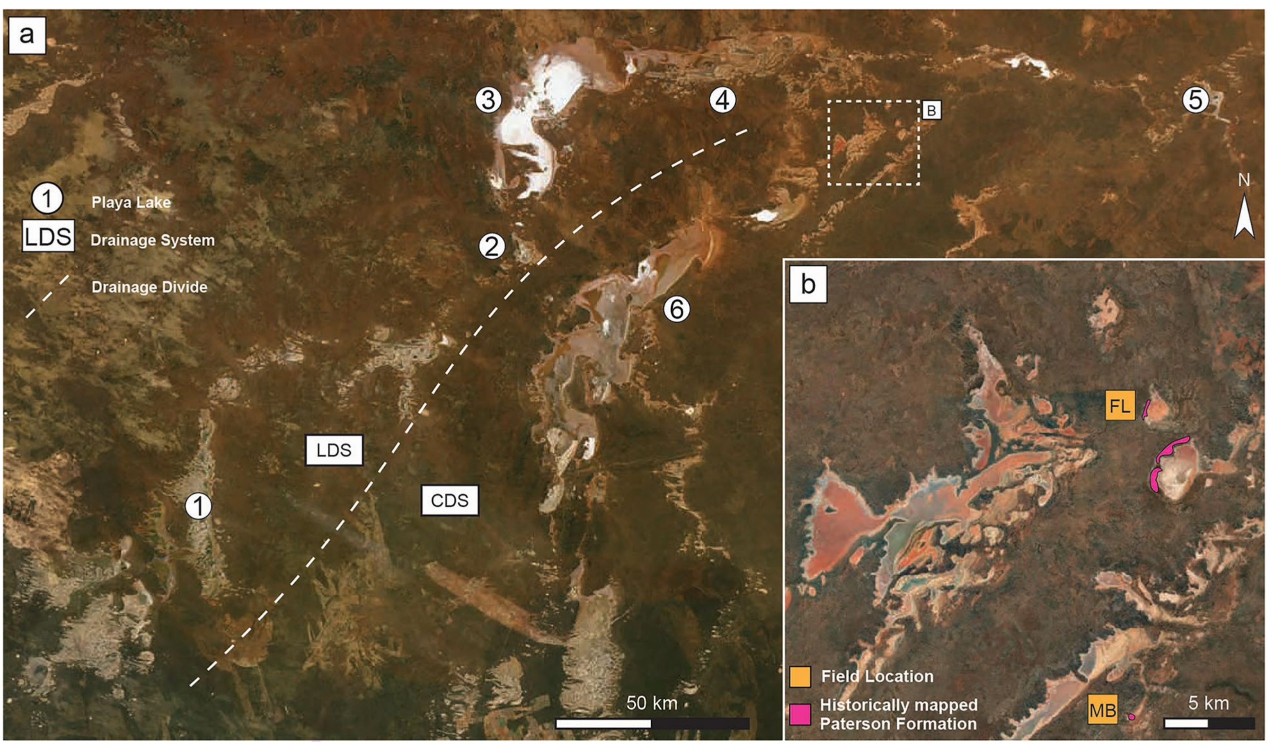

Figure 2. (a) Overview of the area covered by the Lefroy (LDS) and Cowan Drainage systems (CDS). Main playa lakes are numbered. 1, Johnston Lakes; 2, Lake Zot; 3, Lake Lefroy; 4, Lake Randall; 5, Harris Lake; 6, Lake Cowan. Modern inferred drainage divide is represented by the dashed line. (b) Enlarged overview of the field area. FL, Fitzgerald Lagoon; MB, Madoonia Breakaways. Mapped Paterson Formation reproduced from Griffin (1989), Jones (2007) and Sofoulis and Bock (1962).

to long-term tectonic and climatic stability (Anand & Paine, 2002; Magee, 2009). LPIA-related glacial scouring is commonly attributed as responsible for both the low relief of the Yilgarn Craton and the incision of these buried drainage networks (Anand & Butt, 2010; Anand & Paine, 2002; de Broekert & Sandiford, 2005; Magee, 2009; Morgan, 1993; Van de Graaf *et al.*, 1977). Despite this longstanding interpretation of glacial incision, confirmed features of glacial scour and buried tunnel valley networks are only published from two locations within the Eastern Goldfields Region (EGR): Sand King Mine near Kalgoorlie

(Roe Drainage; Figure 1b) and Lancefield North and West near Laverton (Carey Drainage; Figure 1b) (Eyles & de Broekert, 2001; Salama *et al*., 2021).

Additional evidence for glacigene processes in the northern Yilgarn Craton includes glacigene fill of buried drainages, surface erratics and bedrock striations that align with inferred drainage flow directions (Anand & Paine, 2002; Eyles & de Broekert, 2001; Mory *et al*., 2008; Playford, 2001). Thus far, there is little evidence for these processes from the Lefroy Drainage System (LDS). Existing information is limited to geological mapping, where inferred glacigene rocks preserved as outcrop infilling shallow linear depressions, and intersected during subsurface exploration from the lower LDS, were visually correlated with the Paterson Formation (Jones, 2007; Pickard, 2025; Sofoulis, 1965; Sofoulis & Bock, 1962), but no detailed sedimentary facies analysis or paleogeographic studies have been conducted (Sofoulis & Bock, 1962), and interpretations have relied on similarities with published sections inferred to be the Permian Paterson Formation, *e.g.* The Woolnough Hills Diapir reference section (Figure 1a) (Jackson & Van De Graaff, 1981).

Here, we present the first detailed study of these previously mapped deposits of Paterson Formation within the lower reaches of the LDS (Figure 2) to ascertain if the preserved characteristics are consistent with glacigene deposition, and if subsurface morphologies preserved from the LDS are consistent with glacial processes.

Geological setting

The EGR of the Yilgarn Craton comprises the south-southeast/north-northwest-trending Norseman-Wiluna Greenstone Belt: a series of Archean basalts, komatiites and sedimentary basin infill intruded by later-stage granites (Jones *et al*., 2021; Mamuse & Guj, 2011; Oxenburgh *et al*., 2017; Vielreicher *et al*., 2015). The Archean basement is blanketed by regolith deposits of deeply weathered Archean bedrock and recent surface cover, with poorly preserved bedrock outcrop occurrences (Anand & Butt, 2010; Anand & Paine, 2002; Butt *et al*., 1995; Cockbain, 2002). Paleozoic rocks of the EGR are restricted to limited reports on scattered outcrops and subsurface occurrences of the inferred Permian Paterson Formation, interpreted as recording glacigene processes during the LPIA (Eyles & de Broekert, 2001; Jackson *et al*., 1975; Jackson & Van De Graaff, 1981; Jones, 2004; Salama *et al*., 2021, 2022; Salama & Anand, 2017). The EGR is incised by six large-scale drainage systems (Figure 1b) (Beard, 1999; Morgan, 1993; Van de Graaf *et al*., 1977), which, with the exception of consistent Permian basal infill to the north, are infilled with Cenozoic to recent fluvial, lacustrine and shallow marine sedimentary rocks (*e.g.* Broekert, 2002; Clarke *et al*., 2003; Lynham, 2021).

Paterson Formation

Paleozoic sedimentary rocks in the region have historically been assigned to the Paterson Formation. Traves *et al*. (1956) amended the Paterson Range Series of Talbot (1920) to the Paterson Formation to encompass the claystone, siltstone, sandstone and diamictite outcrops in the Canning Basin (Figure 1a).

The Paterson Formation is generally described as a poorly sorted, massive polymictic conglomerate supported by a medium to coarse-grained sandstone matrix, with distinctive glacial features including numerous clasts that are striated, faceted and streamlined into 'bullet-shapes', interbedded with well-bedded lacustrine claystone, siltstone and sandstone (Jackson & Van De Graaff, 1981). The latter authors suggested that owing to lack of flow-direction indicators, the Paterson Formation was deposited under conditions of retreating ice in an outwash fan or fluvio-glacial environment. Direct deposition under basal ice conditions would have resulted in sediments with a preferred orientation of clasts in the direction of ice flow, and pavements of aligned boulders (Boyce & Eyles, 2000). Eyles and de Broekert (2001) proposed that the Paterson Formation within the basal parts of drainages in the northern Yilgarn Craton were deposited by the melting of stagnant ice and subsequent flow down bed rock slopes (*i.e.* flow till).

Correlation of glacial sediments in Western Australia is problematic because the Paterson Formation has effectively become a wastebasket for any vaguely glacigene material that lacks biostratigraphic context. The type section of the Paterson Formation was originally defined as a 35 m section within the Canning Basin (Traves *et al*., 1956); however, it currently lacks the necessary biostratigraphic data to place it within the broader Permian stratigraphy of Western Australia. Consequently, it is now regarded as part of the 'undifferentiated Grant Group' (Backhouse & Mory, 2020). A later reference section of the Paterson Formation was defined by Jackson and Van De Graaff (1981) from an up to 450 m-thick succession of glacio-fluvial, glacio-lacustrine and tillite in the Officer Basin (east of the Yilgarn Craton). This reference section serves as a basis of comparison for glacigene material of the Yilgarn Craton historically assigned to the Paterson Formation. This material occurs: (i) in the subsurface, where it is deposited in glacially scoured valleys and tunnel valleys cut into the bedrock by meltwater beneath the ice sheet, such as at the Sand King mine near Kalgoorlie and the Lancefield West mine near Laverton (Figure 1b) (Eyles & de Broekert, 2001); (ii) in outcrops near Warburton and along the eastern contact of the Yilgarn Craton with the Officer and Gunbarrel basins (Figure 1a) (Kennewell, 1977); and (iii) as extensive 'pavements' of erratics scattered across the surface in the Leonora–Laverton district (Lancefield; Figure 1) (Westaway & Wyche, 1998).

No absolute ages have been reported for material attributed to the Paterson Formation; however, Kemp (1976) recovered a palynological assemblage assigned to the *Nuskoisporites* zone of late Asselian to early Sakmarian age (early Permian), corresponding with the P1 interval of Fielding *et al*. (2023).

According to Backhouse and Mory (2020), the name Paterson Formation should be restricted to scattered outcrop that unconformably overlies Archean basement and associated Proterozoic basins, which forms our justification for naming the rocks from the study area 'Paterson Formation'.

Materials and methods

Field data

The field area comprises two defined locations: Fitzgerald Lagoon and Madoonia Breakaways (Figure 2b; Table 1) represented by the Paterson Formation on the SH51-14 Widgiemooltha 1:250 000 (Griffin & Hickman, 1989) and the 1:100 000 Erayinia map sheets (Jones, 2006) on the Yilgarn Craton, at the downstream confluence of lakes Lefroy and Cowan, where they form a singular drainage and become the downstream third of the LDS (Figure 2) per Bell *et al*. (2012). Mapped outcrop locations of the Paterson Formation occur ~100 km southeast of Kambalda along the western margins of a chain of salt lakes trending southwest to northeast (Figure 3b) and are accessed *via* poorly maintained historical exploration tracks and well-maintained cattle station tracks.

Field-site selection was guided by descriptions from Sofoulis and Bock (1962), Griffin (1989) and Jones (2007) (Figure 2b), their accessibility and their proximity to salt pans within the defined field area. Breakaways along the margins of saltpans within the drainage catchment commonly contain highly weathered rocks (Figure 3), which are otherwise only seen *via* subsurface exploration. The area mapped as Paterson Formation by Griffin and Hickman (1989) in the central field area was explored, but no relevant outcrop was found.

Table 1. Summary of field locations, area, coordinates and the data obtained for this study.

Location	Field area	Facies present	GPS coordinates	CFA	Log?
MD1	Madoonia Breakaways	F2, F3	31°27′37.8″S 122°40′59.3 E	51	Yes
MD2	Madoonia Breakaways	F1, F3	31°27′37.4″S 122°40′46.2″E	50	Yes
MD3	Madoonia Breakaways	F3	31°27′31.8″S 122°41′03.4″E	65	No
MD4	Madoonia Breakaways	F3	31°27′29.4″S 122°41′05.7″E	70	Yes
MD5	Madoonia Breakaways	F3	31°27′37.4″S 122°40′46.2″E	50	No
FL1	Fitzgerald Lagoon	F3	31°19′56.0″S 122°41′28.6″E	11	No

The numbers of clasts analysed for CFA are noted.

The data used in this study were collected from field stratigraphic sections and consist of stratigraphic logs (Figure 4), sedimentary rock descriptions, including grainsize, sorting, bed thickness and bounding contact, field images and hand samples (Figures 5–10). Hand samples were selected and processed for thin-section analyses (Figure 7). Thin-sections were produced by Bob Crossley at Minerex Services (Esperance, Western Australia) and were examined using an Olympus BX53 polarising microscope housed at the Joe Lord Core Library in Kalgoorlie, Western Australia.

Clast form analysis

In sedimentary systems, clasts that have undergone transport may serve as important indicators of paleoenvironmental conditions (*e.g.* Atkins, 2003; Bennett *et al*., 1997; Boulton, 1978; Dobkins & Folk, 1970; Gehringer *et al*., 2025; Molén, 2023). The shape of the clasts can reveal information about provenance as well as changes induced from transport, weathering and erosion. Clast form analysis (CFA) developed by Benn and Ballantyne (1994) can be used to reconstruct the paleoenvironmental history of glacially modified clasts. After glacial affinity was confirmed, a total of 286 clasts were measured for CFA across six sample sites (Figure 8; Table 1). This method involves measuring the a (long), b (intermediate) and c (short) axis of each clast to ascertain the clast shape—blocks, slabs or rods (Sneed & Folk, 1958)—and recording the clast roundness class (Benn, 1990; Benn & Ballantyne, 1994; Matthews, 1987). Finally, the C40 values (% of clasts with c/a ratio <0.4) and RA indices (% of angular and very angular clasts per sample) are plotted against each other to infer the glacial sub-environment of deposition using reference data produced by Benn and Ballantyne (1994) and Lukas *et al*. (2013). Following Lukas *et al*. (2013), care was taken to randomly sample only whole clasts to eliminate bias

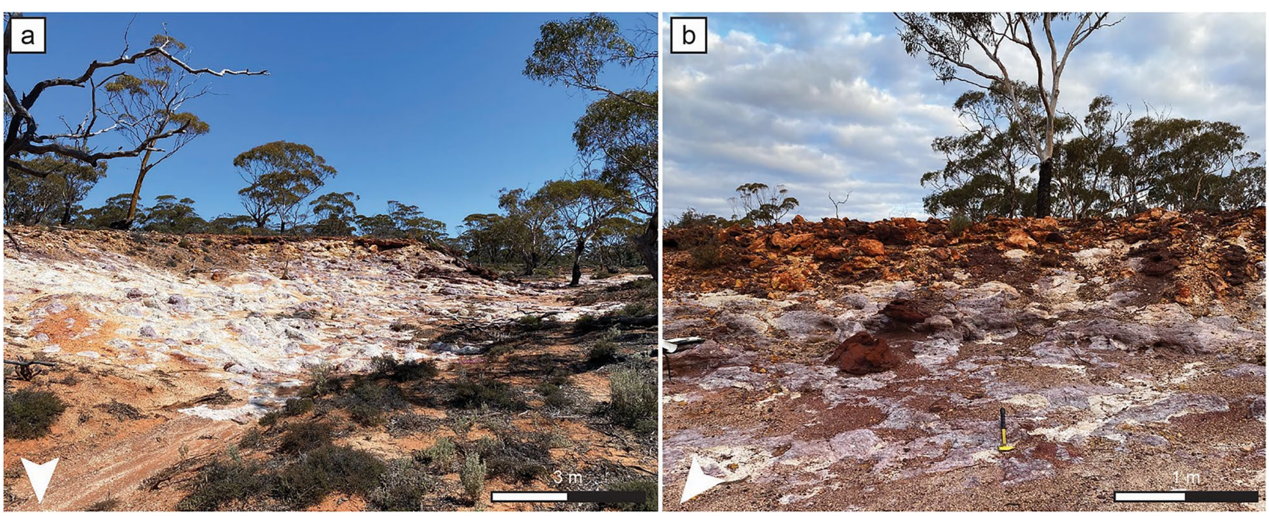

Figure 3. Overview of two locations at Madoonia Breakaways of the typical highly weathered outcrop exposed beneath breakaways encountered within the field area. Arrow is pointing northward.

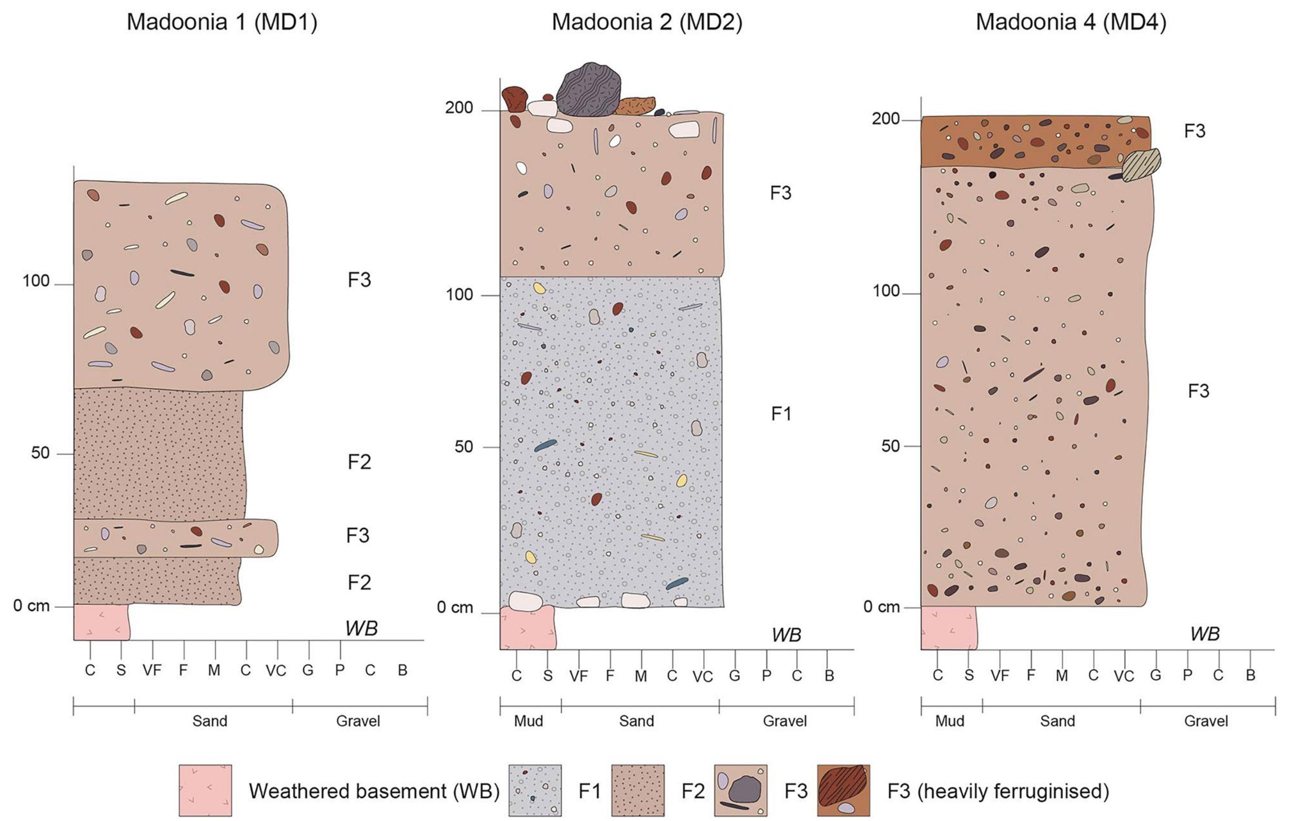

Figure 4. Stratigraphic columns from the studied outcrops at Madoonia Breakaways, Western Australia. Locations are given in Table 1.

regarding shape and/or size, and only large pebbles and cobbles from the field locations were utilised (Figure 6a). Whilst steps were taken to utilise a singular clast lithology to reduce bias in the weathering, erosion and transport history, limited outcrop and exposure meant this was not always feasible; therefore nearly all clasts were quartz-rich lithologies (polycrystalline quartz, foliated granite and gneiss) and are recorded in the supplemental data. Measurements were imported to the TriPlot Excel spreadsheet (Graham & Midgley, 2000) to give the a/b/c axis ratios for interpretation. All measurements and calculations can be found in the supplemental data.

No preserved outcrop occurs at Fitzgerald Lagoon, only a concentrated surface scatter of polymictic clasts with glacigene features, including one used for CFA. Polymictic clasts of inferred glacigene origin also occur in the subsurface. This location has been mapped previously as the Paterson Formation (Griffin, 1989; Sofoulis & Bock, 1962) and is considered an occurrence of F3.

Geomorphology

A depth-to-basement model provided by St Ives Gold Mine (Western Australia) was used to ascertain the subsurface morphology of the LDS with an emphasis on the Lefroy Paleovalley (Figure 11). This 3D model was constructed using Leapfrog Geo 2021.2 and comprises 82 759 drill holes with basement intersects from subsurface drilling. Cross-sections were generated in Leapfrog Geo both longitudinally and across the Lefroy Paleovalley (Figure 12). These cross-sections were compared with published interpretations of glacial morphology from across Australia (English, 2015; Hou *et al*., 2023; Magee, 2009; Tapley, 1988). Additional subsurface data sourced from drilling data found in the West Australian Mineral Exploration Reporting System (WAMEX) from the field area were used to supplement this dataset (Collins, 2013; Pickard, 2025).

Results

Sedimentary facies

The sedimentary rocks in the study location consist of polymictic granule conglomerate, massive sandstone and polymictic pebble conglomerate, comprising three laterally discontinuous sedimentary facies.

Facies 1

Description. Facies 1 (F1; Figure 4) is an inversely graded polymictic granule conglomerate that is laterally discontinuous with a thickness of ~1 m. The lower part of F1 is clast-supported (Figure 5a) and vertically transitions to matrix-supported, with a limited increase in clast size (Figure 5b, c). The basal contact of F1 is irregular and sharply overlays the weathered Archean basement (Figure 5a). Owing to poor outcrop exposure, it is not possible to ascertain whether the undulating contact pre-dates the deposition of F1 or whether it is an erosional feature formed

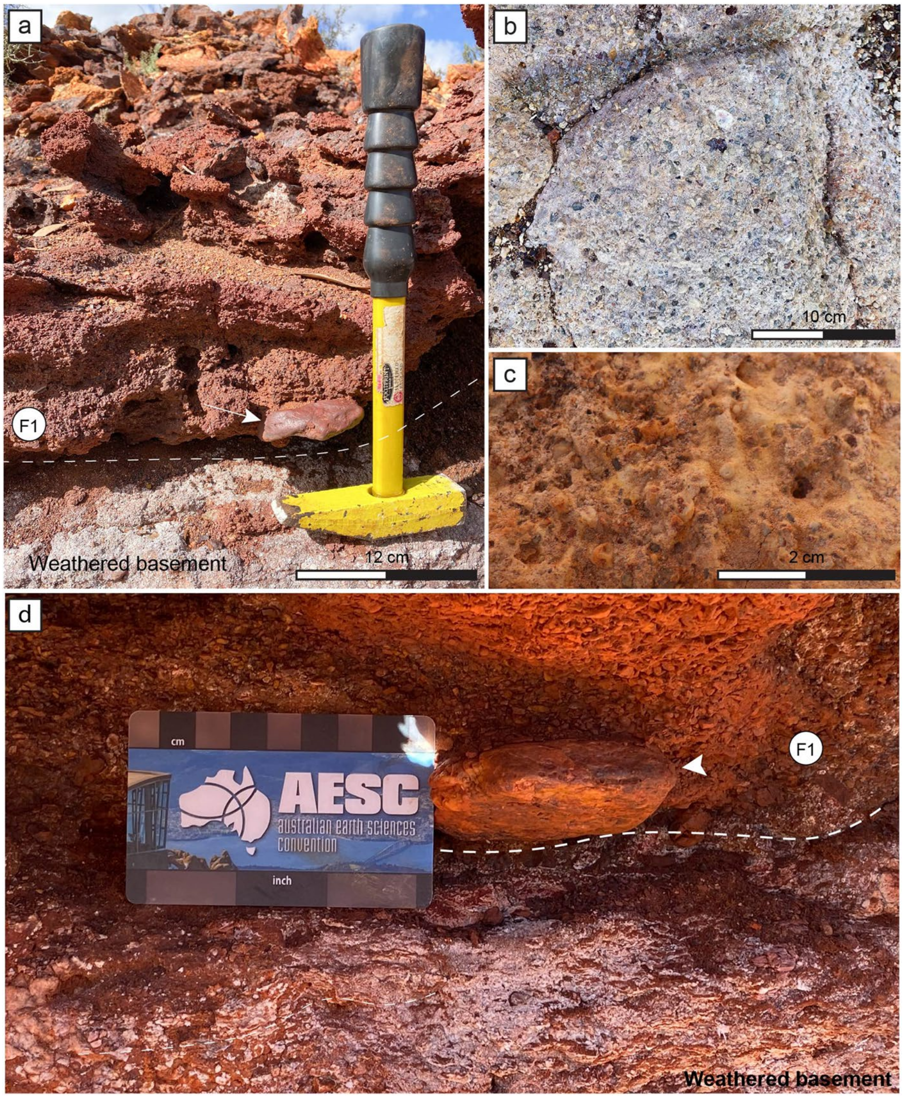

Figure 5. Sedimentary characteristics observed in F1. (a) Contact between the Archean basement (B) and F1. Note the polished and faceted outsized clast of quartz at the base of F1 (see white arrow). (b) Overview of polymictic gravel that comprises F1. (c) Matrix-supported close-up of F1 with range of gravel sized clasts visible. Matrix is high in clay, and gravel clasts are predominantly quartz. (d) Additional image of outsized, flat, polished quartz clast at the base of F1 at the contact with the weathered basement (white arrow).

during emplacement. Grains in F1 are 3–5 mm in diameter and predominantly well rounded (Figure 5b, c), although minor grains of very angular quartz are also present.

The matrix increases up section to ~40% and comprises clay-sized particles with a minor fine-grained quartz component (Figure 5c). Infrequent, large, flat-lying, outsized clasts of elongate, polished and faceted quartz, up to 5 cm across, apparently all orientated southwest–northeast, appear towards the base of F1 (Figure 5a). Along with the matrix increase, the density of large polymictic pebbles also increases up section to 10%. These pebbles reach up to 3 cm long and comprise mainly of polycrystalline quartz with minor lithics, including metamorphosed basement rocks, leucogranite, gneiss, chert and mafic lithologies. Some clasts are highly polished but very rarely display striae. The clasts are randomly orientated and typically elongate with a dominant flat surface displaying a characteristic stoss and lee form (Boulton, 1978). These clasts have also been termed flat-iron, bullet and glacially shaped in the literature (*e.g.* Molén, 2023 and references therein).

Interpretation. F1 was deposited as a fluvio-glacial gravel, in a proglacial environment, proximal to an icesheet. Clast features including polishing (Figure 5a, d), quartz-rich lithologies (Figure 5), distal clasts (Figure 5c) and outsized clasts at the base of F1 (Figure 5a, d) suggest influence by subglacial processes. Polishing of clasts occurs through abrasion at multiple scales until the rock surface becomes optically smooth and can be the dominant abrasion process in the subglacial environment (Benn & Evans, 1998; Siman-Tov *et al.*, 2017), whereas clast striations, indicating subglacial abrasion processes (Boulton, 1982), are very rare. Quartz and granitic clasts comprise the majority of larger pebbles, and owing to their resistant mineralogy, striations on these lithologies are generally uncommon (Benn &

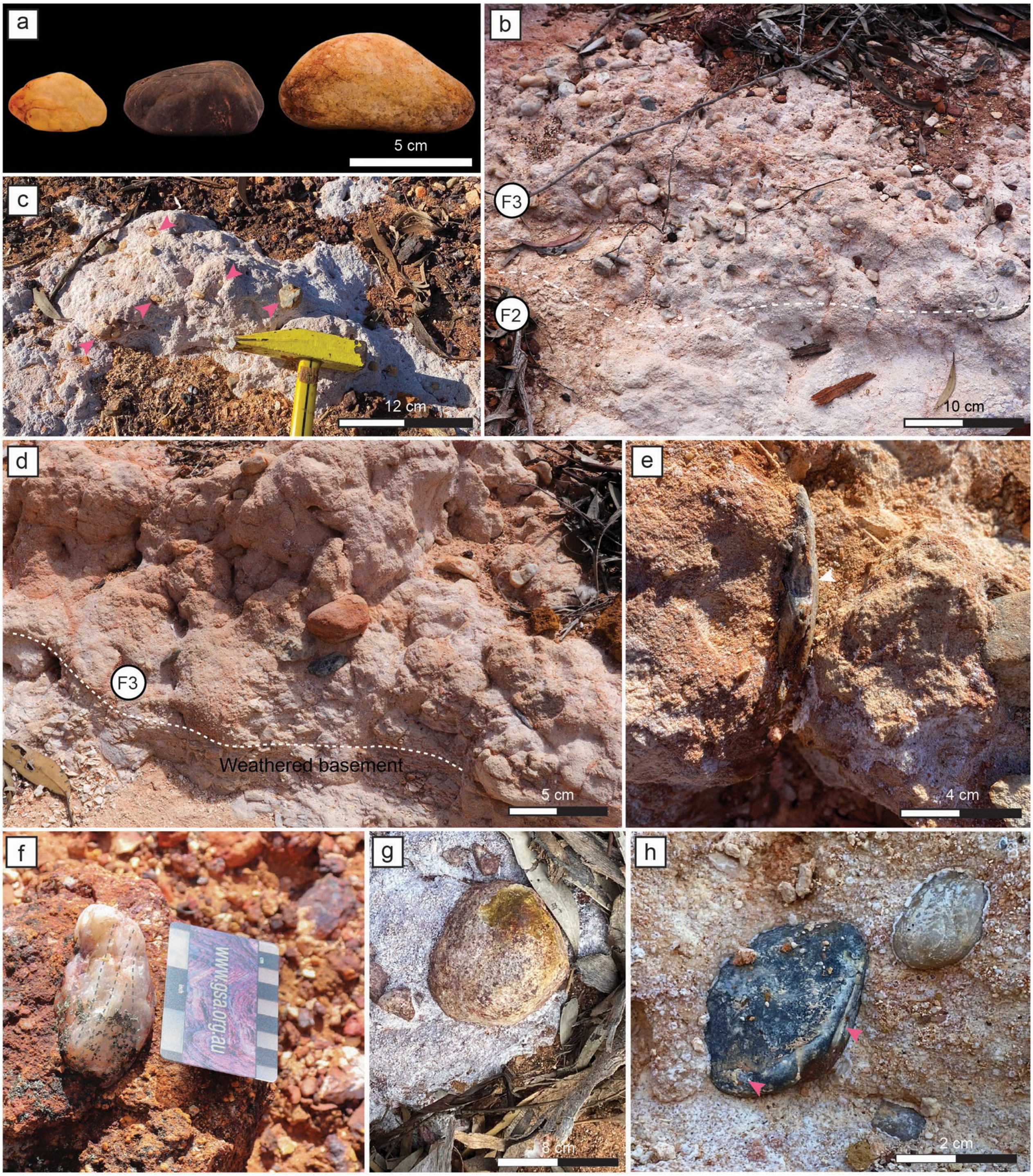

Figure 6. Sedimentary attributes of F2 and F3. (a) Flat-bottomed clasts exhibiting streamlined stoss and lee form. (b) Outcrop section showing the vertical transition from F2 to F3, and the development of a clast pavement up section. (c) Variation of clast size and shape in F3 (pink arrows). (d) Contact between Saprolite (S) and F3. (e) Platy clast from F3. (f) Interpreted striations on a quartz clast. (g) Spherical clast of felsic (possibly granitic) material. (h) Highly polished, optically smooth polymictic pebbles, displaying facets (pink arrows).

Evans, 1998). Stoss and lee clast morphology, as observed in the larger pebbles towards the top of F1, is characteristic of *in situ* subglacial abrasion. This morphology develops from ice sliding over the surface of lodged clasts, and clasts embedded in basal ice sliding over rock (Boulton, 1978; Krüger, 1984, 1994; Sharp, 1982). The large outsized, polished and elongate quartz clasts, flat-lying at the base of F1, show a preferred orientation of southwest–northeast along their long axis, which is inferred to represent the paleoflow direction (Benn & Evans, 1998). These larger clasts likely formed subglacially and were then reworked and deposited by the fluvio-glacial system on the outwash

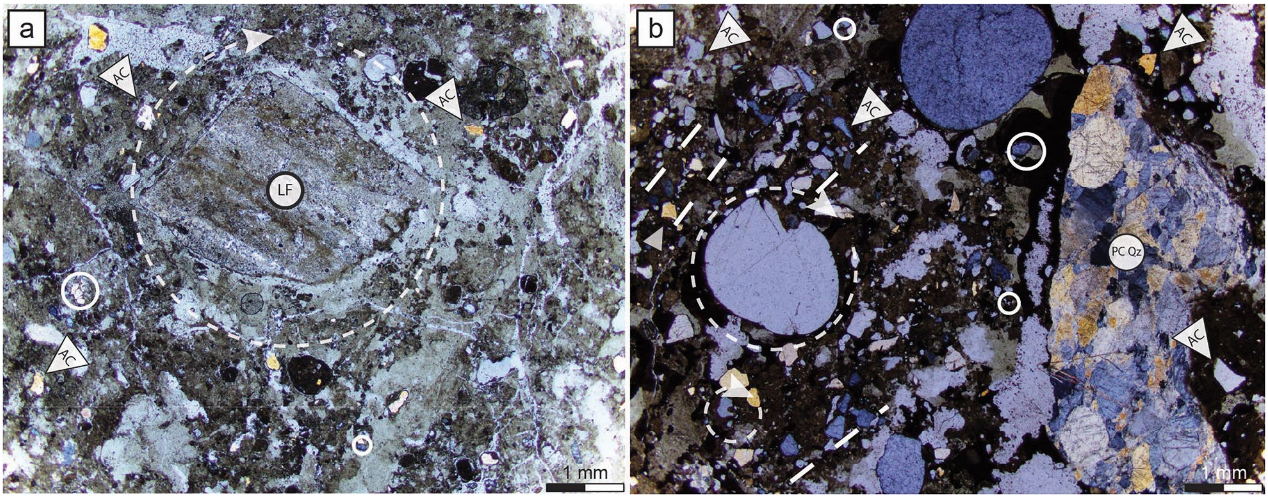

Figure 7. Polarised light thin-section views of (a) F2, showing post-depositional weathering features, and mix of grain shapes in matrix of rock flour and (b) F3, showing clear mix of grain shapes in a 'rock flour' matrix. Rotational structures are marked by open arrows, grain-stacking events by dashed lines, edge–edge crushing events by closed circles. PC Qz, polycrystalline quartz; AC, angular cast.

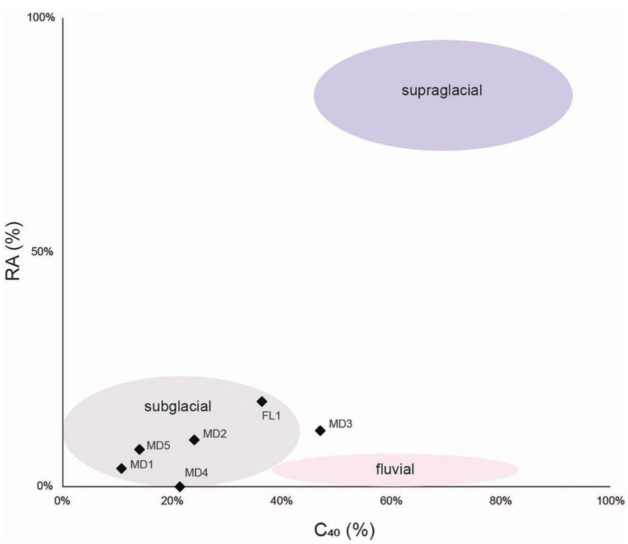

Figure 8. Plotted RA:C40 for Clast Form Analysis in study area. Data presented shows clear subglacial influence of the clasts present. MD3 is an outlier, but as this system is a dynamic environment, some overlap is expected.

plain. The absence of internal crossbedding and the absence of deformation are common characteristics of gravel bars deposited proximal to the terminus of an ice sheet (Rust, 1975).

Additionally, the sorting and grainsize of F1 further indicates its proximity to the ice-margin. Furthermore, the flow velocity appears to decrease up-unit, as evidenced by the increased presence of matrix, but the size of clasts also increases up section. This is likely a product of decreased input to the outwash system from the icesheet (Boyce & Eyles, 2000).

Facies F2

Description. Facies 2 (F2; Figure 4) is a bimodal sandstone made of a framework of coarse angular to sub-angular quartz grains supported by a matrix of clay-sized grains. F2 is up to 40 cm thick and is laterally discontinuous, forming apparent lenses within F3 (below). The contact between F2 and F3 is poorly defined, but F2 appears to grade into F3 with the sudden increase in clast density indicating deposition of F3. Where F2 is in contact with the underlying saprolite, the boundary is undulating.

In thin-section (Figure 7a), F2 exhibits a mix of larger framework grains (2–3 mm) supported by a matrix of smaller grains (<1 mm) and rock flour. There is a clear heterogenic distribution of grain shapes along with edge–edge crushing events, grain stacks and rotational structures.

Interpretation. Whilst there are no macroscale features to interpret F2 beyond 'massive sandstone', microscale structures (Figure 7a) indicate that it has been influenced by stress in a subglacial environment. The matrix, interpreted as rock flour, is characteristic of a glacigene environment formed from the repeated abrasion of material beneath the icesheet until it is essentially pulverised resulting in a very fine-grained matrix, and which typically forms beneath a wet-based glacier (Gunnarsen *et al*., 2019; Haldorsen, 1981; Rampe *et al*., 2022; Vives *et al*., 2025). Edge–edge crushing events, grain stacking and heterolithic grain-shape distribution are characteristic microscale features of subglacial processes and are inconsistent with an outwash plain environment (Le Heron *et al*., 2020; Lister, 1981; Menzies, 2023; Menzies *et al*., 2013, 2016; Menzies & Meer, 2018). Edge–edge crushing events are considered the first microstructure to develop beneath the ice during till formation, from a high but localised strain condition (Menzies, 2023). Grain-stacking features are considered the next stage of deformation after edge–edge events and also represent localised high strain conditions (Menzies, 2023; Menzies *et al*., 2013). Lenses of sand deposited within otherwise

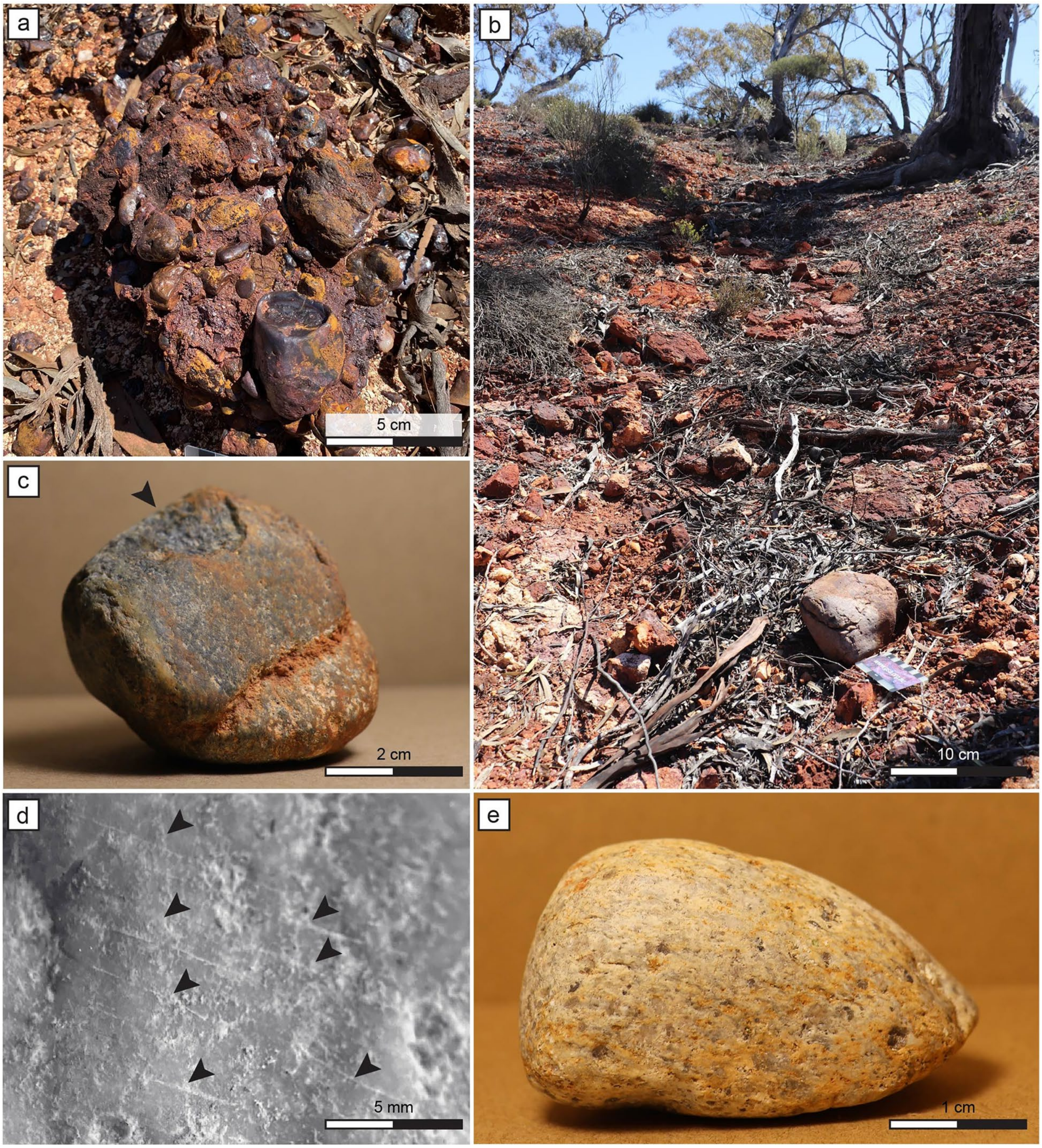

Figure 9. (a) Ironstone conglomerate F3. (b) Gully section Madoonia 4 showing highly weathered F3 in the floor of the gully capped by ironstone conglomerate, F3. Blocks of F3 have weathered out downslope (white arrows). One large, outsized clast is visible of similar dimensions to the boulder lag of F3. (d) Possible striae on a quartz clast. Striae indicated by black arrows. (e) Polished clast with asymmetrical stoss and lee form.

poorly to unsorted glacially influenced sediments are common within sequences derived from the melt-out of debris-rich stagnant ice (Kessler *et al*., 2012 and references therein). F2 may be interpreted as a sand lens within the lower part of a melt-out tillite.

Facies F3

Description. Facies F3 (Figure 4) is polymictic pebbly diamictite that is supported by a silt-rich matrix, at roughly a 50:50 ratio. F3 is capped by a surface lag of polymictic pebbles to boulders (Figure 10) interpreted to have resulted from the collapse and winnowing of matrix of the original F3 and can be described as crudely inversely graded. Clasts average 0.5–5 cm; however, the largest boulders are up to 1 m across. Clast lithology predominantly comprises polycrystalline quartz, foliated granite and gneiss. Other lithologies present include quartz arenite, chert, undifferentiated mafic and ultramafics, banded iron formation and schistose rock. Very rare elongate

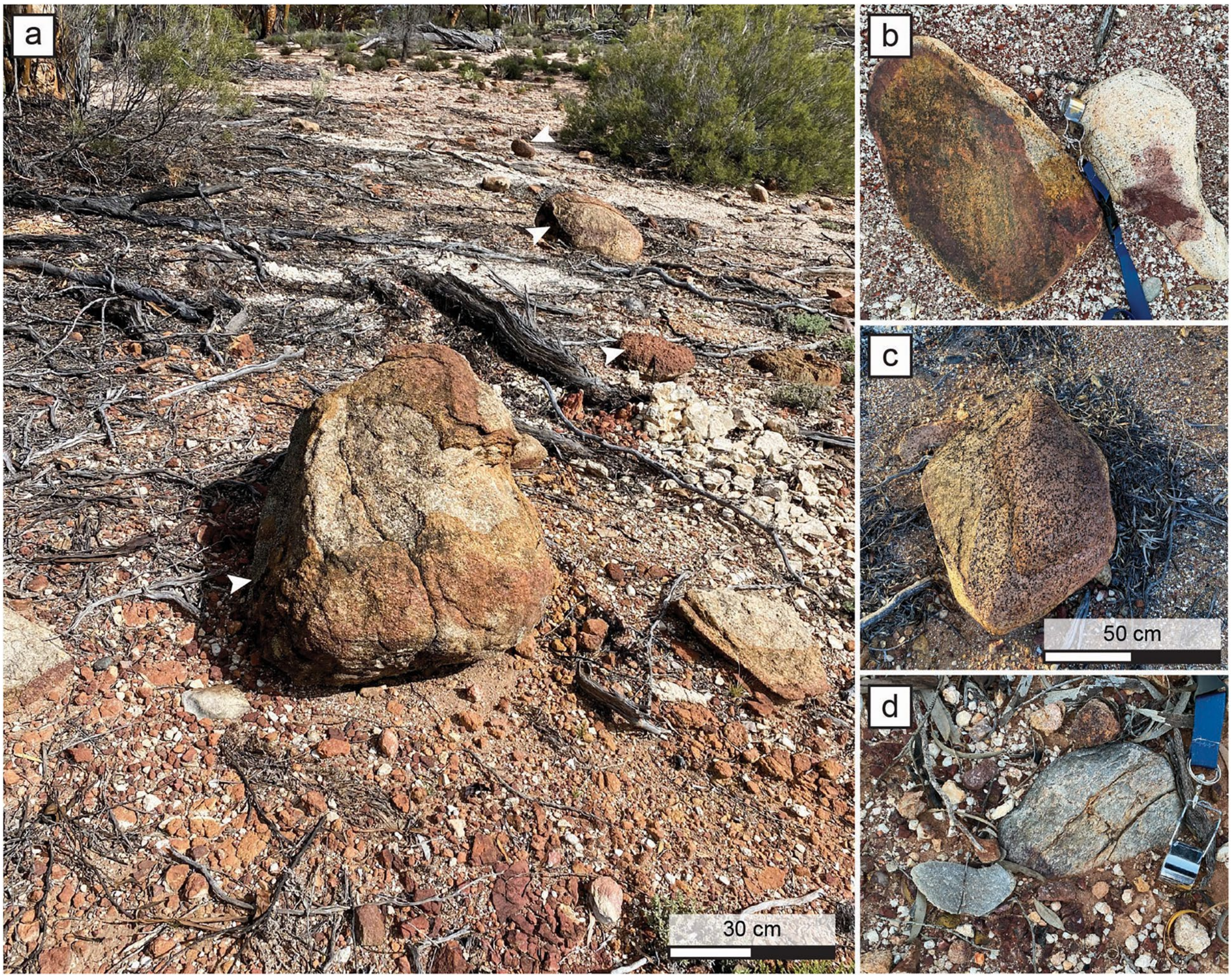

Figure 10. (a) Alignment of large, outsized boulders of granite and gneiss on the surface at Madoonia Breakaways. (b) Large clast of granite displaying stoss and lee form. (c) Large boulder of gneiss showing double stoss and lee form. (d) Cobble of schistose material.

and platy clasts are present (Figure 6e), as are up to 5% angular to very angular clasts. F3 ranges from 40 cm to ~2 m in thickness (Figures 4 and 9e). Most clasts display stoss and lee form (Figures 6a and 9e), with rare, large boulders displaying double stoss and lee form (Figure 10c). More than 60% of the clasts are polished, and faceted clasts are common (Figure 9c), but striae are rarely observed (Figure 9d). The angular clasts within F3 are commonly schistose and mafic lithologies, whereas the highly polished, stoss and lee forms are quartz-dominated lithologies. While F3 includes linear concentrations of clasts both at the base of and throughout F3 (Figures 4 and 6b), no other internal fabric is observed. The F3 contact with F2 is poorly defined to absent. Outcrops are weathered to a bleached buff-peach-grey colour (Figure 6b, d, e). A pebbly ironstone conglomerate discontinuously caps the outcrop at Madoonia Breakaways (*e.g.* Figures 4 and 9a, b); this ironstone conglomerate is a ferruginised variation of F3.

In thin-section, F3 displays a bimodal shape distribution supported by a matrix with poor definition between grains (rock flour). Microfeatures can be observed; edge–edge crushing events, grain stacking and rotational structures are marked where present in Figure 7b. One large clast of foliated granite was thin-sectioned and was shown to be a garnet-bearing leucogranite.

The plotted C_{40} ratio to RA% (Figure 8) places five of six location samples within the subglacial deposition envelope. MD5 sits between the subglacial and fluvial deposition envelopes.

Interpretation. The polymictic mix of lithologies, characteristic stoss and lee form, high number of polished clasts and the C40:RA plots for samples analysed supports the interpretation that F3 was influenced by glacigene processes. Striae, which are commonly associated with glacial abrasion, are mostly absent from F3. The dominant quartz-rich, resistant mineralogy of the lithologies within F3 led to polishing becoming the dominant subglacial abrasion process (Benn & Evans, 1998). Heterogenic size distribution of grains within a rock flour matrix is common in the subglacial environment and forms from the repeated mechanical abrasion of bedrock by glacial activity beneath a wet-based glacier (Gunnarsen *et al*., 2019; Haldorsen, 1981; Rampe *et al*., 2022).

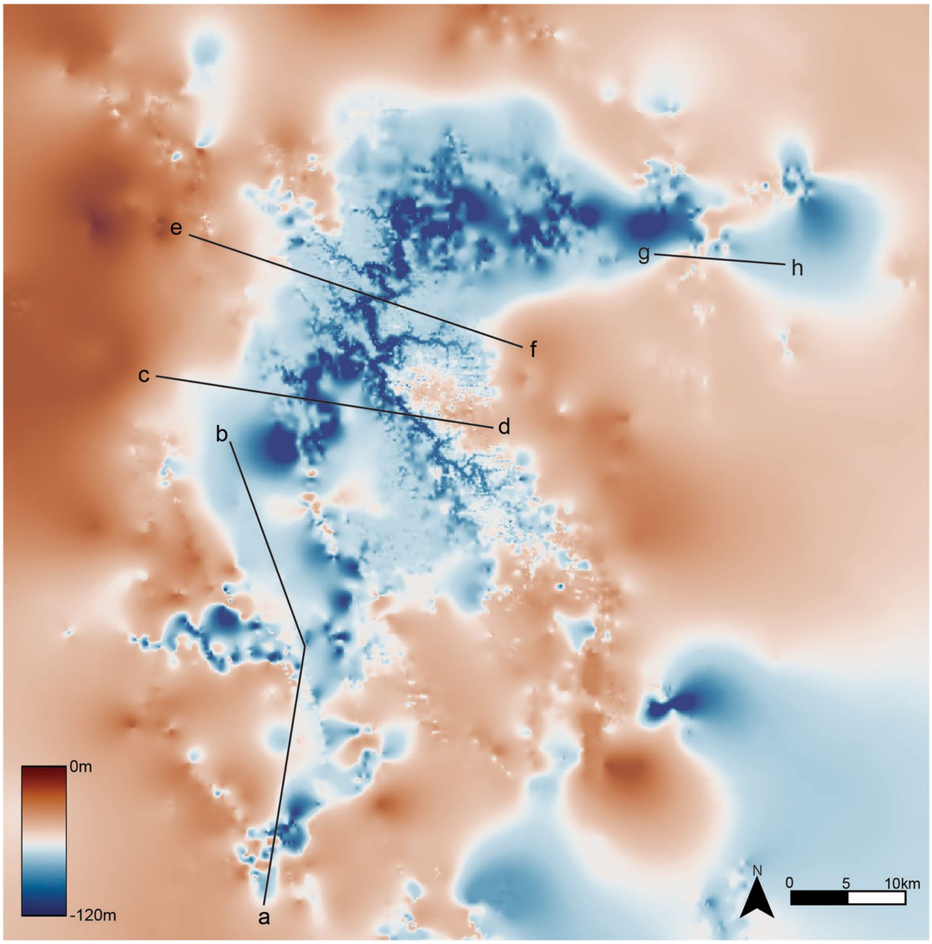

Figure 11. Depth-to-basement model for the Lefroy Paleovalley (Lake Lefroy; Figure 2). Cross-section locations (Figure 12) are marked. Colour ramp from Crameri (2023).

The largest boulders of F3 are gneissic lithologies that do not occur as basement rocks in the local area. Whilst foliated granites do outcrop on the Widgiemooltha map sheet, granites that contain garnet as an accessory mineral are not known, except from the Albany Fraser Orogen >60 km to the south suggesting a distal origin and long transport history (Griffin, 1989; Griffin & Hickman, 1989). Additionally, banded iron formation is not known from the immediate catchment area, with the closest known source the Santa Claus Formation outcropping near the northwest shore of Lake Randall (Figure 2) (Griffin & Hickman, 1989). CFA plots (Figure 8) indicate subglacial deposition. The outlier, MD5, may be a feature of mixed lithology, or a feature of dynamic glacigene depositional environments causing an overlap of envelopes (Bennett *et al*., 1997; Lukas *et al*., 2013).

Microscale processes visualised in thin-section (Figure 7b) represent deformation processes in the subglacial environments (Brodzikowski & Vanloon, 1987; Le Heron *et al*., 2020; Menzies *et al*., 2016). Edge–edge crushing of grains represents the first stage of subglacial sediment formation, whereas grain stacking develops when strain is released (Menzies, 2023; Menzies *et al*., 2013; Menzies & Meer, 2018). Rotation structures, which are also observed in thin-section of F3 (Figure 7b), are common in subglacial tills indicating plastic deformation processes (Menzies, 2023; Menzies *et al*., 2016). The preserved characteristics infer that F3 may have been deposited as part of the melt-out of stagnant, debris-rich wet-based ice (Bennett & Glasser, 1996; Boyce & Eyles, 2000; Eyles & de Broekert, 2001). The crude inverse grading of F3 further supports this conclusion.

Depth-to-basement model

Depth-to-basement (Figure 11) was determined as the depth at which weathered crystalline basement (saprock and/or saprolite) or fresh crystalline, Archean rock (if there was a stripped regolith profile) was intersected during drilling. From this model, four cross-sections were created—two across valley and two longitudinal, to ascertain the bottom profile morphology (Figure 12). The Cenozoic fluvial inset valley can be seen as the darkest blue on Figure 11.

Longitudinal cross-sections a–b and g–h (Figures 11 and 12) show an undulating bottom morphology. Across-valley sections c–d and e–f (Figures 11 and 12) show a broad, flat U-shaped valley with a V-shaped fluvial inset channel. The width-to-height ratios of these cross-sections is high, and section c–d shows an asymmetrical profile. These observations are consistent with glacial valley morphology (Harbor, 1989; White, 1972).

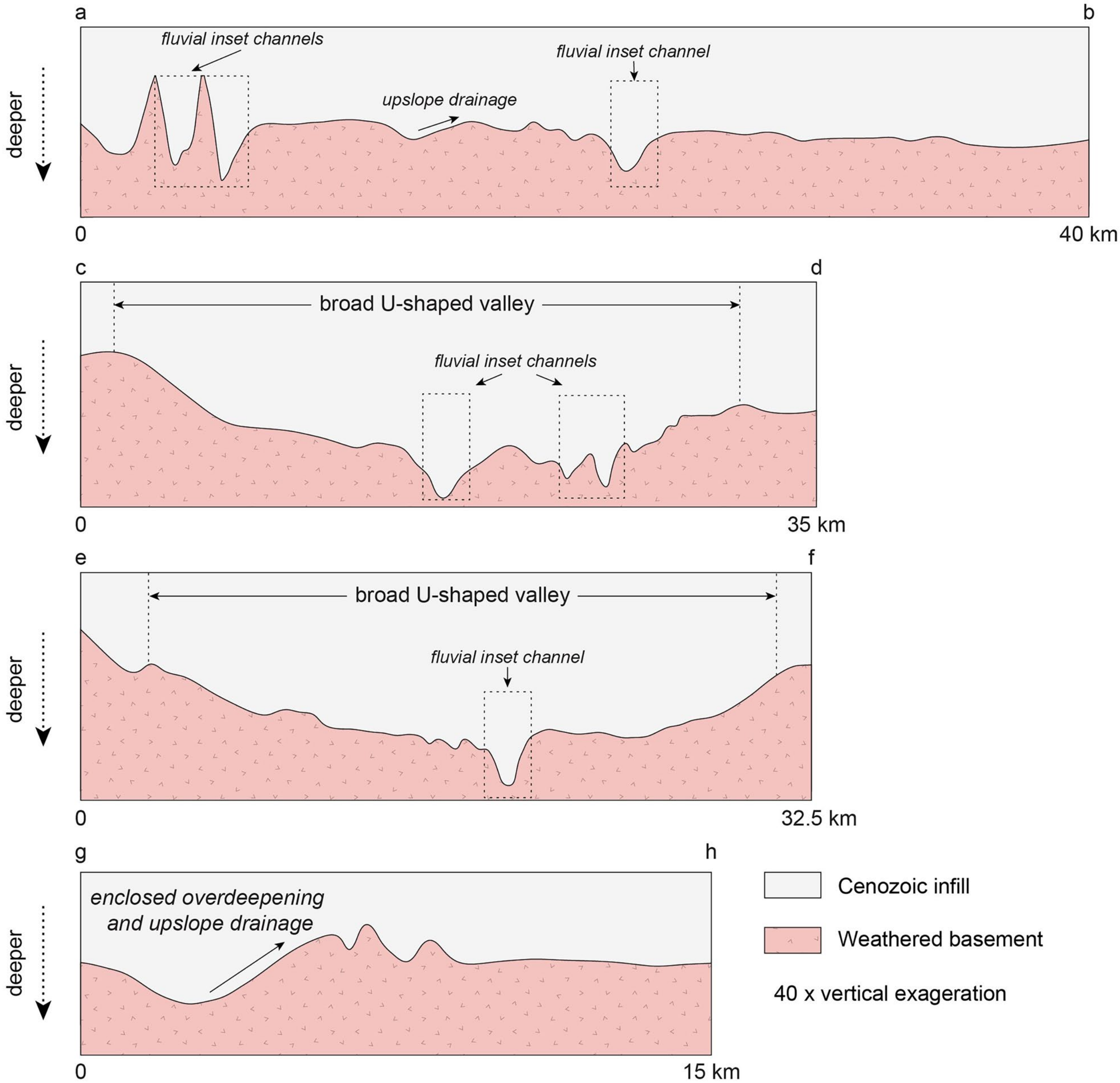

Figure 12. Cross-sections (see their location on Figure 11) produced from the depth-to-basement model. The cross-sections show an undulating floor in longitudinal section and broad, U-shaped cross-sections with V-shaped inset valleys. Note the different scale for each cross-section. Vertical exaggeration is 40× on each section.

Within the study area, historical exploration drilling intersected glacigene material at a maximum depth of 112 m (Figures 13 and 14). This unit is up to 42 m thick, containing 'mafic and felsic rounded transported pebbles' (Pickard, 2025) and visually matches F3 described above. Historical drilling data (Collins, 2013) were used to produce a crude west-to-east cross-section of the basement profile and buried Permian fill from this area (Figure 14). This cross-section shows an irregular, asymmetrical Archean basement topography. This morphology is consistent with buried examples of tunnel valleys from Canada (*e.g.* Atkinson *et al*., 2013). Permian glacigene material unconformably deposited above Archean basement and beneath more commonly reported Eocene paleochannel infill further evidences a primary glacial scour origin for the LDS.

Discussion

Paleoenvironmental interpretation

The sedimentary facies preserved at Madoonia Breakaways and Fitzgerald Lagoon are interpreted as deposited proximal to the proglacial environment on an outwash plain (F1) and within the ice-contact environment from the melt-out of 'dead-ice' with the release of stagnant, debris-rich ice (F2 and F3). This is comparable with the environment inferred from buried tunnel valleys to the north of the LDS (Eyles & de Broekert, 2001).

Facies 1 is interpreted as an outwash gravel deposited under decreasing velocity and decreased input into the outwash system (Boyce & Eyles, 2000). The matrix increase up section, along with increasing presence of larger polymictic clasts, suggests

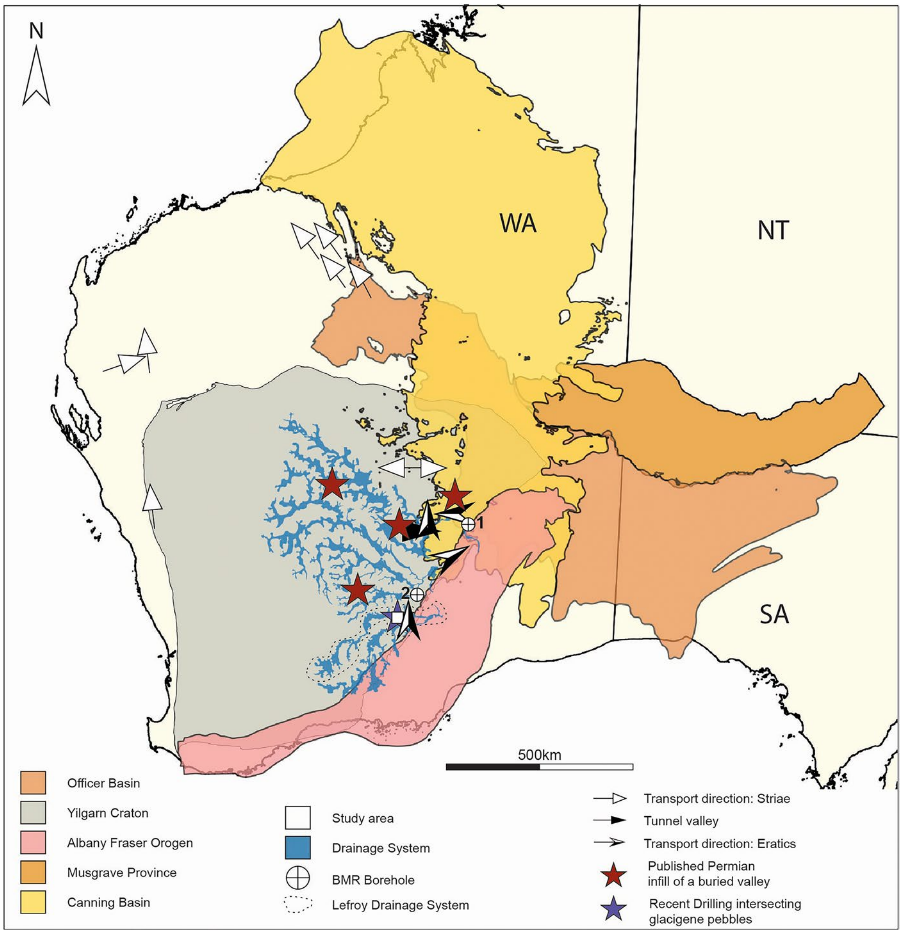

Figure 13. Regional map showing ice-growth/movement directions and borehole locations discussed in the text. BMR1, BMR Rason; BMR2, Cundeelee 4. Data compiled from this study, Jackson and Van De Graaff (1981), Jackson *et al*. (1975), Jones (2004), Playford (2001) and Salama *et al*. (2022).

that the outwash system was captured and buried by ice-contact melt-out facies (F2 and F3). The discontinuous nature of F1 is interpreted as a feature of poor outcrop preservation, but it may also be interpreted as outwash gravel infilling existing channels on an outwash plain (also termed a sandur in some literature) (Kjær *et al*., 2004; Miall, 1996).

Facies 2, when interpreted in association with F3, is inferred to be deposited as sandy lenses within a lower section of melt-out tillite, and F3 is interpreted as tillite deposited by the *in situ* melting of debris-rich, stagnant ice at the base of an icesheet during glacial retreat (Paul & Eyles, 1990). This interpretation is evidenced by: (i) the distal nature and form of clasts (including stoss and lee morphology, and up to 60% polished clasts), interpreted as influenced by ice during their formational history; (ii) the poor sorting and crude inverse grading of F3 with an overall increase in clast size; and (iii) the microscale features indicating subglacial influence (*e.g.* Menzies, 2023; Menzies & Meer, 2018). CFA from F3 supports the interpretation of subglacial influence. An ice-contact environment with subglacial influence is preferred over a purely subglacial environment of deposition, as there is a lack of clast alignment within F3 (Boyce & Eyles, 2000). No proximal outcropping source for many of the polymictic pebbles or boulders from any of the facies can be inferred, nor are the lithologies present in the subsurface (Griffin & Hickman, 1989). Outcropping basement in the local area comprises heavily weathered Archean bedrock (saprock) with minor outcrops of metamorphosed mafic rocks (basalt and basaltic pillow lava) associated with the Norseman-Wiluna Greenstone Belt and the metasedimentary rocks and evaporites of the Woodline sub-basin (Griffin & Hickman, 1989). Proterozoic basement rocks across the entire Yilgarn Craton contain large, sheared quartz veins, and these are the likely source of the majority of the polycrystalline quartz clasts. Owing to the widespread distribution of these quartz veins, the provenance of clasts cannot be narrowed down. The largest clasts and boulders are gneissic and garnet-bearing lithologies. The closest known provenance of these lithologies is the Albany Fraser Orogen >60 km to the south (Griffin, 1989).

Fluvial or glacial? Morphology interpretation

The characteristic effect of fluvial and glacial processes on landscape evolution is established consensus. Typically, fluvial systems produce V-shaped valleys, and glacial systems U-shaped valleys (Bennett & Glasser, 1996; Fryirs & Brierley, 2012; Glasser & Bennett, 2004; Kaufmann, 1872; Montgomery, 2002; Prasicek *et al*., 2014). Major landforms produced from glacial erosion can

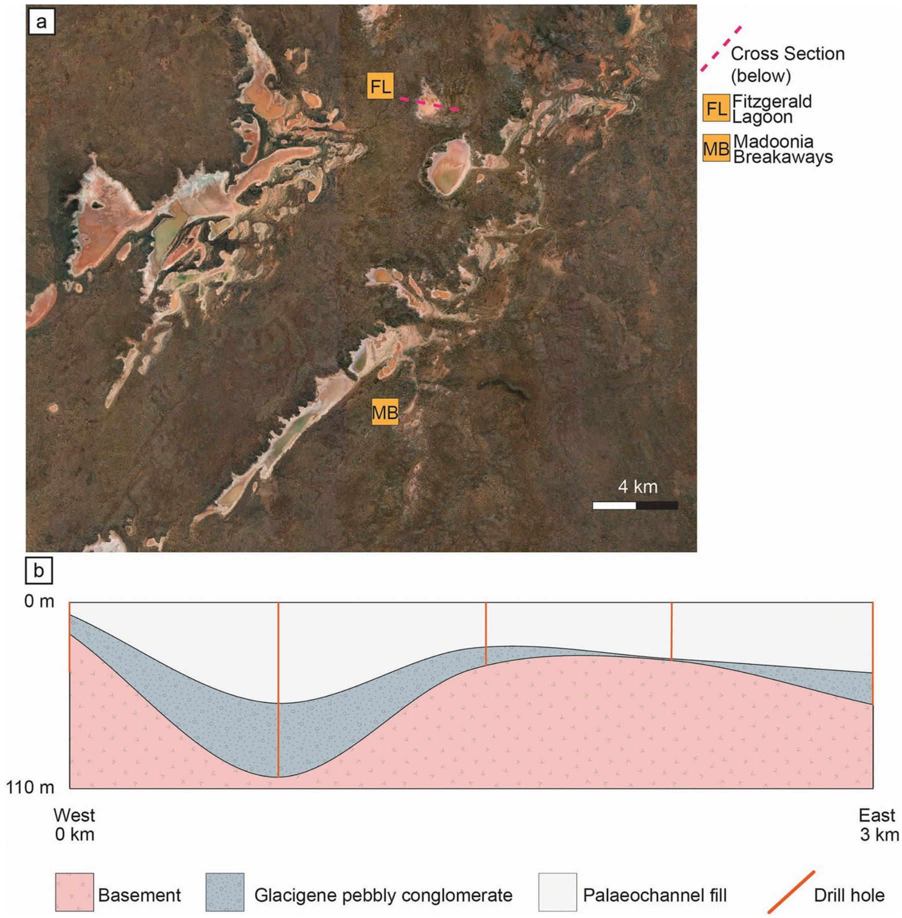

Figure 14. (a) Satellite image showing the location of cross-section created from open-source drilling data at Fitzgerald Lagoon. (b) Cross-section created from open-source drilling data from Fitzgerald Lagoon.

be hidden in the landscape and preserved as buried features (Magrani *et al.*, 2020). Glacially scoured landscapes also exhibit other distinct morphology that defines their glacial origin including (i) undulating longitudinal profiles, (ii) narrowing and widening phases and (iii) sections of overdeepening. They may also contain buried tunnel valleys cut beneath the scour surface and are commonly infilled with glacigene sediments (Anderson *et al.*, 2006; Hooke, 1991; Kaufmann, 1872; Kehew *et al.*, 2012).

The LDS comprises a series of interconnected ellipsoidal primary valleys, connected by thin channels that are incised perpendicular to the Archean bedrock fabric (*e.g.* Jones, 2024 and references therein). The LDS exhibits widening and narrowing phases with a hierarchical control (larger ellipsoidal lakes giving way to thinner, elongated 'finger' lakes) (Figure 2). There are no apparent bedrock lithological or structural controls to account for this morphology, and the LDS cuts through the grain and structural control of the underlying Archean greenstone belt (Gresham & Loftus-Hills, 1981). The interconnected ellipsoidal valleys along with their widening and narrowing phases and lack of lithological control are characteristic of glaciated valleys and subglacial abrasion and erosion by meltwater under pressure (Eyles, 1983; Stewart *et al.*, 2012, 2013). Undulating longitudinal bottom profiles, as seen in the study area (Figure 12), may form from meltwater erosion from turbulent flows in pressurised subglacial channels beneath the ice sheet (Grau Galofre *et al.*, 2018; Greenwood *et al.*, 2007; Kehew *et al.*, 2012; Sissons, 1961). As subglacial meltwater gradients are controlled by the hydraulic gradient and not the topography, the resulting high-pressure flow can move upslope as well as down (Kehew *et al.*, 2012; Stewart *et al.*, 2012, 2013). However, this may also be a feature of differential erosion of the underlying Archean bedrock from the icesheet activity (*e.g.* Harbor, 1995).

An enclosed overdeepening where Lake Lefroy becomes Lake Randall (Figure 2) down to ~120 m has been extrapolated (Figures 11 and 12; line g–h). This enclosed overdeepening also coincides with a direction change in the system from northeast trending to due east.

Overdeepening with respect to the thalweg, is a characteristic process that occurs during glacial incision (Carrivick *et al.*, 2016; Haeberli *et al.*, 2016; Patton *et al.*, 2016). Overdeepenings or closed topographic depressions develop from a combination of direct glacial abrasion and plucking (the process by which large bedrock blocks are moved 'down glacier') (Hooke, 1991; Iverson, 2012), as well as erosion by subglacial meltwater (*e.g.* Beaud *et al.*, 2016; Herman *et al.*, 2011; Ugelvig *et al.*, 2018). Overdeepenings in formerly glaciated landscapes are commonly occupied by lakes (Hooke, 1991) and in the geological record may be infilled with glacially influenced diamictite or lacustrine sediments (*e.g.* Ghienne *et al.*, 2007). To the north of the main trunk of the LDS, within the Ponton Creek Paleovalley, which connects the lower reaches of the LDS with the Roe Drainage System (Van de Graaf *et al*., 1977), a described overdeepening has been extrapolated from drilling data (Bunting & Van De Graaff, 1977). The Cundeelee 4 Borehole (Figure 13; BMR 2) sampled an enclosed depression infilled with ~200 m of Permian-aged glacio-lacustrine sediments (clay and silt with drop stones) before intersecting Archean basement. This is inferred to have been incised from LPIA-related processes (Bunting & Van De Graaff, 1977; Jackson *et al*., 1975; Jackson & Van De Graaff, 1981).

The preserved features suggest the Lefroy Paleovalley can be considered a now-buried glacial erosional feature and potentially a tunnel valley. These are distinct linear features subglacially incised into both unlithified sediment and bedrock by meltwater processes in areas of flat or low relief (Bennett & Glasser, 1996; Kehew *et al*., 2012), such as beneath a glacially scoured landscape. Their reported scale ranges up to several hundreds of kilometres in length, tens of kilometres wide and up to hundreds of metres deep (Dietrich *et al*., 2025; Kehew *et al*., 2012; Livingstone & Clark, 2016). Valley base profile variations of 50–100 m are observed in a confirmed Pleistocene buried tunnel valley network in Denmark (Jørgensen & Sandersen, 2006), whilst overdeepenings beneath the Antarctic ice sheet have been reported up to 300 m (Patton *et al*., 2016), so the variations within the LDS (Figures 11, 12 and 14; Jackson *et al*., 1975) are consistent with the published literature.

Whilst Pleistocene examples are well preserved (*e.g.* Lipka, 2025), pre-Pleistocene examples are more difficult to recognise, especially when buried. LPIA examples have been recognised from southern Africa (Dietrich *et al*., 2025), Western Australia (Al-Hinaai & Redfern, 2014; Eyles & de Broekert, 2001), South Australia (Alley *et al*., 2026) and Brazil (Tedesco *et al*., 2016). The interpreted LPIA Western Australian example (Eyles & de Broekert, 2001) comprises basins up to 3 km wide incised up to 80 m deep into the underlying Archean bedrock, cutting across bedrock structure and infilled with tillite deposited from the melt-out of stagnant, debris-rich basal ice. Whilst this example is narrower than the LDS example, the morphology is directly comparable. LPIA-related processes recorded from South Australia include 'significant troughs' from the Troubridge, Arckaringa, Cooper, Pedrika and Nadda basins (Alley *et al*., 2026). These troughs are up to tens of kilometres wide and hundreds of kilometres long, in fitting with the morphology of the LDS. They are, however, up to 1 km deep—far deeper than what is seen in the LDS. The deepest part of the LDS is the interpreted enclosed basin at Cundeelee 4 ~ 220 m deep. This drillhole was situated at an RL of 325 m, and ~11 km away from Archean bedrock outcrops at an RL of up to 400 m (Bunting & Van De Graaff, 1977). This illustrates the irregular bedrock erosional surface on the Yilgarn Craton, showing that direct comparisons of morphology between drainages is difficult. Further north, glacigene infill in buried drainage systems is recorded as up to 189 m thick and deposited in asymmetrical basins (Salama & Anand, 2017).

Overall, the preserved glacigene facies and buried morphology suggest that the incision of LDS is related to a series of glacial processes, in line with the common hypothesis that the buried drainage systems of the Yilgarn Craton are the result of ice scour processes during the LPIA. The later fluvial inset valleys are marked by V-shaped 'insets' within the broader glacially associated morphology (Figure 12). Future subsurface drilling and review of historical drilling records and geophysical data sets may further narrow down these glacial abrasion processes.

Regional correlations and age affinities

Thus far, no conclusive radiometric dating has been undertaken on the LDS tillite. Dating for inferred equivalent units is based on palynology from the 1960s and 1970s, with the geographically closest material examined being the Bureau of Mineral Resources (BMR) Rason 1 borehole (Figure 13), ~300 km to the north (Kemp, 1976), which inferred a Sakmarian (early Permian) age. This age is consistent with published observations of a P1 glaciation in Western Australia (299–290 Ma) (Fielding *et al*., 2023). The orientation of the linear depressions infilled with glacigene material at Madoonia Breakaways (Figure 2), along with the inferred provenance of gneiss from the Albany Fraser Orogen ~60 km to the south, matches recorded data for ice sheet growth and retreat directions during the LPIA on the West Australian Shield (Alley *et al*., 2026; Eyles & de Broekert, 2001; Mory *et al*., 2008; Playford, 2001; Traves *et al*., 1956; Veevers, 2006) (Figure 13). Additionally, detrital zircon studies from Lancefield (Figure 1) (Salama *et al*., 2022) imply provenance from the south and east (Albany Fraser Orogen and Musgrave Province).

The units observed at Madoonia Breakaways and Fitzgerald Lagoon broadly resemble the descriptions of tillite within the Paterson Formation of the Officer Basin where these are moderately to poorly sorted, coarse-grained and containing distal clasts (Jackson & Van De Graaff, 1981). Similar tillite facies, along with glacio-lacustrine facies, have been identified in (i) the subsurface of the Roe and Rebecca drainage systems to the north of the LDS (Figure 1) (Eyles & de Broekert, 2001; Griffin, 1989; Jackson & Van De Graaff, 1981; Laws, 1980; Salama *et al*., 2021; Salama & Anand, 2017; Sofoulis, 1965; Sofoulis & Bock, 1962); (ii) infilling both shallow and deep inferred Permian valleys near Gruyere, northeast of the Lancefield tunnel valley (Salama *et al*., 2022); and (iii) outcropping as fluvio-glacial facies and isolated boulder lag to the north of the study area (Jackson & Van De Graaff, 1981; Westaway & Wyche, 1998). In combination, this evidence infers regionally equivalent conditions existed on the West Australian Shield during the LPIA with the terminus of the ice sheet located along the margin of the Yilgarn Craton and Officer Basin. Debate remains as to whether the glaciation of the West Australian Shield was contiguous or composed of multiple smaller ice centres.

Evidence from the LPIA of South Australia (Alley *et al*., 2013, 2026; Bourman & Alley, 1999; Normington *et al*., 2018), which broadly matches the sedimentary facies described in this study, are described as 'flow till' (equivalent to the melt-out facies described above) and reported as glacigene diamictite interbedded with sand. However, much of the evidence from South

Australia suggests a single continuous ice sheet up to 4 km thick moving to the north-northwest depositing extensive proglacial sediments (*e.g.* Alley *et al*., 2026) at this time.

Evidence for a brief Early Cretaceous glaciation has been discovered within the southern Eromanga Basin in Queensland and the Flinders Ranges, South Australia (Alley *et al*., 2020, 2026). Whilst visually the units described from Madoonia Breakaways and Fitzgerald Lagoon have broad similarities with sedimentary facies from the glacigene Paterson Formation as described by Jackson and Van De Graaff (1981), and interpreted subsurface morphologies infer alike glacigene processes across the Yilgarn Craton, the lack of biostratigraphic data available prevents a certain correlation with the LPIA. Future work should look to dating these sections.

Despite the widespread preservation of glacial facies and erosional features present in drainage systems to the north of the study area (Eyles & de Broekert, 2001; Salama *et al*., 2021; Salama & Anand, 2017), and extensive subsurface exploration of the LDS, the only known glacial sediments from this drainage are those described above, inferred glacial pebbles from the subsurface to the north of the field area (Pickard, 2025) and subsurface glacio-lacustrine and fluvio-glacial sediments described close to the terminus of the drainage by Jackson and Van De Graaff (1981). This scarcity of preservation is likely due to the extensive inundation by marine transgressions and subsequent erosion of the upper reaches of the LDS during the Cenozoic (Clarke, 1994b, 1994a; Clarke *et al*., 1996, 2003).

Conclusions

This study provides the first detailed description of glacial facies that occur in the LDS, Western Australia. The preserved facies consist of gravelly sandstone, massive sandstone and pebbly diamictite deposited proximal to the terminus of an ice sheet. The facies described in this study are broadly similar to the glacially inferred lithofacies of the Paterson Formation intersected in the subsurface to the north of the LDS, infilling incised valleys and outcropping as thin veneers on the Archean basement along the margins of the Yilgarn Craton and Officer Basin, Western Australia. This study shows broad U-shaped primary valley morphology making up the LDS, with V-shaped fluvial inset valleys. Collectively, these facies and morphology are analogous to regional occurrences of glacial material across the Yilgarn Craton.

Acknowledgements

The authors would like to thank Ngadju Native Title Aboriginal Corporation for access to their Determination; Madoonia Downs for access to their pastoral lease tracks; St Ives Gold Mine and Gold Fields Australia for access to drillhole data, field safety monitoring and loaning of a vehicle to access the field sites; Oleg Koudashev, Leo Speed, Jay Stafford and Kayla Piggott for their assistance in the field; Paul Dirks, Bob Crossley, Alicia Verbeeten, Douglas Benn, Amanda Owen and Gresley Wakelin-King for their discussion and technical assistance during the length of this project. We warmly thank Neville Alley and Antoine Dillinger for their constructive reviews that greatly improved the manuscript.

Author contributions

CRediT: **L. Lynham**: Conceptualization, Formal analysis, Investigation, Methodology, Project administration, Writing – original draft, Writing – review & editing; **E. Knutsen**: Conceptualization, Supervision, Validation, Writing – review & editing; **G. Smith**: Supervision, Writing – review & editing; **R. Vaucher**: Supervision, Validation, Visualization, Writing – review & editing.

Disclosure statement

No potential conflict of interest was reported by the authors.

Use of artificial intelligence

No generative AI was used in the production of this manuscript. AI was used as a tool to refine grammar during the editing stages.

Funding

This research was supported by an Australian Government Research Training Program Scholarship and in-kind support from St Ives Gold Mine (Gold Fields Australia).

ORCID

L. Lynham http://orcid.org/0000-0002-0110-5379
E. Knutsen http://orcid.org/0000-0003-2646-2214
G. Smith http://orcid.org/0000-0002-6773-0425
R. Vaucher http://orcid.org/0000-0003-3051-4128

Data availability statement

All the data are available in the manuscript and the supplemental data.

References

Al-Hinaai, J., & Redfern, J. (2014). The late Carboniferous basal Grant Group unconformity, Canning Basin, Australia: A complex surface recording glacial tectonic and halotectonic processes. *Australian Journal of Earth Sciences*, *61*(5), 703–717. https://doi.org/10.1080/08120099.2014.921241

Alley, N. F., Bourman, R. P., & Milnes, A. R. (2013). Late Paleozoic Troubridge Basin sediments on Kangaroo Island. *South Australia. MESA Journal*, *70*(3), 18–37.

Alley, N. F., Flint, R. B., Bourman, R. P., Ives, L. R. W., Hou, B., & Francis, J. E. (2026). Major paleogeographic and paleoclimatic changes during the late Paleozoic, Early Cretaceous and Cenozoic of central Australia and their influence on recycling of sediments. *Australian Journal of Earth Sciences*, *73*(1), 1–83. https://doi.org/10.1080/08120099.2025.2582129

Alley, N. F., Hore, S. B., & Frakes, L. A. (2020). Glaciations at high-latitude Southern Australia during the Early Cretaceous. *Australian Journal of Earth Sciences*, *67*(8), 1045–1095. https://doi.org/10.1080/08120099.2019.1590457

Anand, R. R., & Butt, C. R. M. (2010). A guide for mineral exploration through the regolith in the Yilgarn Craton, Western Australia. *Australian Journal of Earth Sciences*, *57*(8), 1015–1114. https://doi.org/10.1080/08120099.2010.522823

Anand, R. R., & Paine, M. (2002). Regolith geology of the Yilgarn Craton, Western Australia: Implications for exploration. *Australian Journal of Earth Sciences*, *49*(1), 3–162. https://doi.org/10.1046/j.1440-0952.2002.00912.x

Anderson, R. S., Molnar, P., & Kessler, M. A. (2006). Features of glacial valley profiles simply explained. *Journal of Geophysical Research: Earth Surface*, *111*(F1), F01004. https://doi.org/10.1029/2005JF000344

Atkins, C. B. (2003). *Characteristics of Striae and Clast shape in glacial and non-glacial environments* [unpublished PhD thesis]. Victoria University of Wellington.

Atkinson, N., Andriashek, L. D., & Slattery, S. R. (2013). Morphological analysis and evolution of buried tunnel valleys in northeast Alberta, Canada. *Quaternary Science Reviews*, *65*, 53–72. https://doi.org/10.1016/j.quascirev.2012.11.031

Backhouse, J., & Mory, A. J. (2020). Mid-Carboniferous–Lower Permian palynology and stratigraphy, Canning Basin, Western Australia. *Geological Survey of Western Australia*, *Report 207*, 148 p.

Beard, J. S. (1999). Evolution of the river systems of the south-west drainage division, Western Australia. *Journal of the Royal Society of Western Australia*, *82*(4), 147–164.

Beaud, F., Flowers, G. E., & Venditti, J. G. (2016). Efficacy of bedrock erosion by subglacial water flow. *Earth Surface Dynamics*, *4*(1), 125–145. https://doi.org/10.5194/esurf-4-125-2016

Bell, J. G., Kilgour, P. L., English, P. M., Woodgate, M. F., Lewis, S. J., & Wischusen, J. D. H. (2012). *WASANT Palaeovalley Map - Distribution of Palaeovalleys in Arid and Semi-arid WA–SA–NT.* (First Edition), scale: 1:4 500 000.

Benn, D. I. (1990). *Scottish late-glacial moraines: Debris supply, genesis and significance* [unpublished PhD thesis]. University of St Andrews.

Benn, D. I., & Ballantyne, C. K. (1994). Reconstructing the transport history of glacigenic sediments: A new approach based on the co-variance of clast form indices. *Sedimentary Geology*, *91*(1-4), 215–227. https://doi.org/10.1016/0037-0738(94)90130-9

Benn, D. I., & Evans, D. J. A. (1998). *Glaciers & glaciation* (1st ed.). Edward Arnold.

Bennett, M. R., & Glasser, N. F. (1996). *Glacial geology: Ice sheets and landforms*. John Wiley.

Bennett, M. R., Hambrey, M. J., & Huddart, D. (1997). Modification of clast shape in high-Arctic glacial environments. *Journal of Sedimentary Research*, *67*(3), 550–559. https://doi.org/10.1306/D42685CC-2B26-11D7-8648000102C1865D

Boulton, G. S. (1978). Boulder shapes and grain-size distributions of debris as indicators of transport paths through a glacier and till genesis. *Sedimentology*, *25*(6), 773–799. https://doi.org/10.1111/j.1365-3091.1978.tb00329.x

Boulton, G. S. (1982). Processes and Patterns of Glacial Erosion. In D. R. Coates (Ed.) *Glacial geomorphology* (pp. 41–87). Springer. https://doi.org/10.1007/978-94-011-6491-7_2

Bourman, R. P., & Alley, N. F. (1999). Permian glaciated bedrock surfaces and associated sediments on Kangaroo Island, South Australia: Implications for local Gondwanan ice-mass dynamics. *Australian Journal of Earth Sciences*, *46*(4), 523–531. https://doi.org/10.1046/j.1440-0952.1999.00720.x

Boyce, J. I., & Eyles, N. (2000). Architectural element analysis applied to glacial deposits: Internal geometry of a late Pleistocene till sheet, Ontario, Canada. *Geological Society of America Bulletin*, *112*(1), 98–118. https://doi.org/10.1130/0016-7606(2000)112<98:Aeaatg>2.0.Co;2

Brodzikowski, K., & van Loon, A. J. (1987). A systematic classification of glacial and periglacial environments, facies and deposits. *Earth-Science Reviews*, *24*(5), 297–381. https://doi.org/10.1016/0012-8252(87)90061-4

Broekert, P. (2002). *Origin of Tertiary Inset Valleys and their Fills, Kalgoorlie, Western Australia* [unpublished PhD thesis]. Australian National University. https://doi.org/10.25911/5d778508e7815

Bunting, J. A., & Van De Graaff, W. J. E. (1977). *Explanatory notes on the Cundeelee 1:250 000 geological sheet, Western Australia. Geological Survey of Western Australia*, 25. Western Australia, Department of Energy, Mines, Industry Regulation and Safety.

Butt, C. R. M., Anand, R. R., & Smith, R. E. (1995). *Regolith geology and exploration geochemistry in the Yilgarn Craton, Western Australia*. CSIRO Division of Exploration and Mining.

Caputo, M. V., de Melo, J. H., Streel, M. G., Isbell, J. L., & Isbell, J. L. (2008). Late Devonian and Early Carboniferous glacial records of South America. In C. R. Fielding, T. D. Frank (Eds.). *Late Devonian and Early Carboniferous glacial records of South America* (pp. 161–173). Geological Society of America Special. Paper 441. https://doi.org/10.1130/2008.2441(11)

Carrivick, J. L., Davies, B. J., James, W. H. M., Quincey, D. J., & Glasser, N. F. (2016). Distributed ice thickness and glacier volume in southern South America. *Global and Planetary Change*, *146*, 122–132. https://doi.org/10.1016/j.gloplacha.2016.09.010

Clarke, J. D. A. (1994a). Evolution of the Lefroy and Cowan palaeodrainage channels, Western Australia. *Australian Journal of Earth Sciences*, *41*(1), 55–68. https://doi.org/10.1080/08120099408728113

Clarke, J. D. A. (1994b). Geomorphology of the Kambalda Region, Western Australia. *Australian Journal of Earth Sciences*, *41*(3), 229–239. https://doi.org/10.1080/08120099408728132

Clarke, J. D. A., Bone, Y., & James, N. P. (1996). Cool-water carbonates in an Eocene palaeoestuary, Norseman formation, Western Australia. *Sedimentary Geology*, *101*(3-4), 213–226. https://doi.org/10.1016/0037-0738(95)00066-6

Clarke, J. D. A., Gammon, P. R., Hou, B., & Gallagher, S. J. (2003). Middle to Upper Eocene stratigraphic nomenclature and deposition in the Eucla Basin. *Australian Journal of Earth Sciences*, *50*(2), 231–248. https://doi.org/10.1046/j.1440-0952.2003.00995.x

Cockbain, A. E. (2002). Regolith geology of the Yilgarn Craton—Introduction. *Australian Journal of Earth Sciences*, *49*(1), 1–1. https://doi.org/10.1046/j.1440-0952.2002.00913.x

Collins, J. E. (2013). *Combined Annual Report on Erayinia Project—C85/2011 for period 23 September 2012 to 22 September 2013*. *Integra Mining*.

Crameri, F. (2023). *Scientific Colour Ramps*. Zenodo. https://doi.org/10.5281/zenodo.1243862

Crowell, J. C., & Frakes, L. A. (1971). Late Palaeozoic glaciation of Australia. *Journal of the Geological Society of Australia*, *17*(2), 115–155. https://doi.org/10.1080/00167617108728730

de Broekert, P., & Sandiford, M. (2005). Buried inset-valleys in the Eastern Yilgarn Craton, Western Australia: Geomorphology, age, and allogenic control. *The Journal of Geology*, *113*(4), 471–493. https://doi.org/10.1086/430244

Dietrich, P., Guillocheau, F., Douillet, G. A., Griffis, N. P., Baby, G., Le Héron, D. P., Barrier, L., Mathian, M., Montañez, I. P., Robin, C., Gyomlai, T., Kettler, C., & Hofmann, A. (2025). The glacial paleolandscapes of Southern Africa: The legacy of the Late Paleozoic Ice Age. *Earth Surface Dynamics*, *13*(3), 495–529. https://doi.org/10.5194/esurf-13-495-2025

Dillinger, A., Vaucher, R., & Haig, D. W. (2022). Refining the depositional model of the Lower Permian Carynginia Formation in the northern Perth Basin; anatomy of an ancient mouth bar. *Australian Journal of Earth Sciences*, *69*(1), 135–151. https://doi.org/10.1080/08120099.2021.1928751

Dobkins, J. E., & Folk, R. L. (1970). Shape development on Tahiti-Nui. *Journal of Sedimentary Research*, *40*(4), 1167–1203. https://doi.org/10.1306/74D72162-2B21-11D7-8648000102C1865D

English, P. (2015). *Paterson Province Investigation for the Palaeovalley Groundwater Project.* Geoscience Australia Record 2012/007. http://www.ga.gov.au/corporate_data/73671/Rec2012_007.pdf

Eyles, N. (1983). *Glacial geology: An introduction for engineers and earth scientists* (1st ed.). Pergamon Press.

Eyles, N., & de Broekert, P. (2001). Glacial tunnel valleys in the Eastern Goldfields of Western Australia cut below the Late Paleozoic Pilbara ice sheet. *Palaeogeography Palaeoclimatology Palaeoecology*, *171*(1-2), 29–40. https://doi.org/10.1016/S0031-0182(01)00265-6

Eyles, N., Mory, A. J., & Backhouse, J. (2002). Carboniferous–Permian palynostratigraphy of west Australian marine rift basins: Resolving tectonic and eustatic controls during Gondwanan glaciations. *Palaeogeography, Palaeoclimatology, Palaeoecology*, *184*(3-4), 305–319. https://doi.org/10.1016/s0031-0182(02)00260-2

Eyles, C. H., Mory, A. J., & Eyles, N. (2003). Carboniferous–Permian facies and tectono-stratigraphic successions of the glacially influenced and rifted

Carnarvon Basin, Western Australia. *Sedimentary Geology*, *155*(1-2), 63–86. https://doi.org/10.1016/S0037-0738(02)00160-4

Fielding, C. R., Frank, T. D., & Birgenheier, L. P. (2023). A revised, late Palaeozoic glacial time-space framework for eastern Australia, and comparisons with other regions and events. *Earth-Science Reviews*, *236*, 104263. https://doi.org/10.1016/j.earscirev.2022.104263

Fielding, C. R., Frank, T. D., Birgenheier, L. P., Rygel, M. C., Jones, A. T., & Roberts, J. (2008). Stratigraphic imprint of the Late Palaeozoic Ice Age in eastern Australia: A record of alternating glacial and nonglacial climate regime. *Journal of the Geological Society*, *165*(1), 129–140. https://doi.org/10.1144/0016-76492007-036

Fryirs, K. A., & Brierley, G. J. (2012). *Geomorphic Analysis of River Systems: An Approach to Reading the Landscape*. Wiley-Blackwell. https://doi.org/10.1002/9781118305454

Gehringer, E. R., Ferrari, G., Morgan, A. M., & Palucis, M. C. (2025). Using clast morphometry to reconstruct basaltic sediment transport history. *Journal of Geophysical Research: Planets*, *130*(11), e2025JE009154. https://doi.org/10.1029/2025JE009154

Ghienne, J-F., Le Heron, D. P., Moreau, J., Denis, M., & Deynoux, M. (2007). The Late Ordovician glacial sedimentary system of the North Gondwana platform. In M. J. Hambrey, P. Christoffersen, N. F. Glasser & B. Hubbard (Eds.), *Glacial sedimentary processes and products* (pp. 295–319). John Wiley & Sons, Incorporated. https://doi.org/10.1002/9781444304435.ch17

Glasser, N. F., & Bennett, M. R. (2004). Glacial erosional landforms: Origins and significance for palaeoglaciology. *Progress in Physical Geography: Earth and Environment*, *28*(1), 43–75. https://doi.org/10.1191/0309133304pp401ra

Graham, D. J., & Midgley, N. G. (2000). Graphical representation of particle shape using triangular diagrams: An Excel spreadsheet method. *Earth Surface Processes and Landforms*, *25*(13), 1473–1477. https://doi.org/10.1002/1096-9837(200012)25:13<1473::Aid-Esp158>3.0.Co;2-C

Grau Galofre, A., Jellinek, A. M., Osinski, G. R., Zanetti, M., & Kukko, A. (2018). Subglacial drainage patterns of Devon Island, Canada: Detailed comparison of rivers and subglacial meltwater channels. *The Cryosphere*, *12*(4), 1461–1478. https://doi.org/10.5194/tc-12-1461-2018

Greenwood, S. L., Clark, C. D., & Hughes, A. L. C. (2007). Formalising an inversion methodology for reconstructing ice-sheet retreat patterns from meltwater channels: Application to the British Ice Sheet. *Journal of Quaternary Science*, *22*(6), 637–645. https://doi.org/10.1002/jqs.1083

Gresham, J. J., & Loftus-Hills, G. D. (1981). The geology of the Kambalda nickel field, Western Australia. *Economic Geology*, *76*(6), 1373–1416. https://doi.org/10.2113/gsecongeo.76.6.1373

Griffin, T. J. (1989). Explanatory notes on the Widgiemooltha 1:250 000 geological sheet, Western Australia. *Geological Survey of Western Australia*, *1989/4*, 88.

Griffin, T. J., & Hickman, A. H. (1989). *Widgiemooltha WA Sheet SH51-14 1:250000*. Geological Survey of Western Australia.

Gunnarsen, K. C., Jensen, L. S., Gómez-Muñoz, B., Rosing, M. T., & de Neergaard, A. (2019). Glacially abraded rock flour from Greenland: Potential for macronutrient supply to plants. *Journal of Plant Nutrition and Soil Science*, *182*(5), 846–856. https://doi.org/10.1002/jpln.201800647

Haeberli, W., Linsbauer, A., Cochachin, A., Salazar, C., & Fischer, U. H. (2016). On the morphological characteristics of overdeepenings in high-mountain glacier beds. *Earth Surface Processes and Landforms*, *41*(13), 1980–1990. https://doi.org/10.1002/esp.3966

Haldorsen, S. (1981). Grain-size distribution of subglacial till and its relation to glacial scrushing and abrasion. *Boreas*, *10*(1), 91–105. https://doi.org/10.1111/j.1502-3885.1981.tb00472.x

Harbor, J. M. (1995). Development of glacial-valley cross sections under conditions of spatially variable resistance to erosion. *Geomorphology*, *14*(2), 99–107. https://doi.org/10.1016/0169-555x(95)00051-1

Harbor, J. M. (1989). Early Discoverers XXXVI: W.J. McGee on glacial erosion laws and the development of glacial valleys. *Journal of Glaciology*, *35*(121), 419–425. https://doi.org/10.3189/S0022143000009357

Herman, F., Beaud, F., Champagnac, J-D., Lemieux, J-M., & Sternai, P. (2011). Glacial hydrology and erosion patterns: A mechanism for carving glacial valleys. *Earth and Planetary Science Letters*, *310*(3–4), 498–508. https://doi.org/10.1016/j.epsl.2011.08.022

Hooke, R. L. (1991). Positive feedbacks associated with erosion of glacial cirques and overdeepenings. *Geological Society of America Bulletin*, *103*(8), 1104–1108. https://doi.org/10.1130/0016-7606(1991)103<1104:P-faweo>2.3.Co;2

Hou, B., Petts, A., Krapf, C., Irvine, J., Stoian, L., Heath, P., Reed, G., & Foss, C. (2023). *Remapping the paleovalley systems of the central-western Gawler Craton, South Australia*. Geological Survey of South Australia. Report Book 2023/00043.

Hyde, W., Crowley, T., Tarasov, L., & Peltier, W. R. (1999). The Pangean ice age: Studies with a coupled climate-ice sheet model. *Climate Dynamics*, *15*(9), 619–629. https://doi.org/10.1007/s003820050305

Isbell, J. L. (2010). Environmental and paleogeographic implications of glaciotectonic deformation of glaciomarine deposits within Permian strata of the Metschel Tillite, southern Victoria Land, Antarctica. In O. R. López-Gamundí & L. A. Buatois (Eds.), *Late Paleozoic Glacial Events and Postglacial Transgressions in Gondwana* (pp. 81–100). Geological Society of America. Special Paper 468. https://doi.org/10.1130/2010.2468(03)

Isbell, J. L., Henry, L. C., Gulbranson, E. L., Limarino, C. O., Fraiser, M. L., Koch, Z. J., Ciccioli, P. L., & Dineen, A. A. (2012). Glacial paradoxes during the late Paleozoic ice age: Evaluating the equilibrium line altitude as a control on glaciation. *Gondwana Research*, *22*(1), 1–19. https://doi.org/10.1016/j.gr.2011.11.005

Isbell, J. L., Miller, M. F., Wolfe, K. L., & Lenaker, P. A. (2003). Timing of late Paleozoic glaciation in Gondwana; was glaciation responsible for the development of Northern Hemisphere cyclothems?. In M. A. Chan & A. W. Archer (Eds.), *Extreme depositional environments: Mega end members in geologic time* (pp. 5–24). *Geological Society of America. Special Paper 370*. https://doi.org/10.1130/0-8137-2370-1.5

Iverson, N. R. (2012). A theory of glacial quarrying for landscape evolution models. *Geology*, *40*(8), 679–682. https://doi.org/10.1130/G33079.1

Jackson, M. J., & Van De Graaff, W. J. E. (1981). *Geology of the Officer Basin, Western Australia*. Geoscience Australia. Record 206.

Jackson, M. J., Van De Graaff, W. J. E., & Boegli, J. C. (1975). *Shallow Stratigraphic Drilling in the Officer Basin, Western Australia, 1972*. Bureau of Mineral Resources, Geology and Geophysics. 1975/049.

Jones, J. A. (2004). *Geology of the Wongawol 1:100 000 sheet: Western Australia Geological Survey*. 1:100 000 Geological Series Explanatory Notes, 28.

Jones, J. A. (2006). *Erayinia, W.A Sheet 3435: Western Australia Geological Survey*. 1:100 000 Geological Series.

Jones, J. A. (2007). Geology of the Erayinia 1:100 000 sheet Western Australia Geological Survey. *1:100 000 Geological Series Explanatory Notes*, 37.

Jones, S. A. (2024). 2730–2670 Ma rifting triggers sagduction prior to the onset of orogenesis at *ca* 2650 Ma: Implications for gold mineralisation, Eastern Goldfields, Western Australia. *Australian Journal of Earth Sciences*, *71*(5), 647–672. https://doi.org/10.1080/08120099.2024.2337773

Jones, S. A., Cassidy, K. F., & Davis, B. K. (2021). Unravelling the D event: Evidence for early granite-up, greenstone-down tectonics in the Eastern Goldfields, Western Australia. *Australian Journal of Earth Sciences*, *68*(1), 1–35. https://doi.org/10.1080/08120099.2020.1755364

Jørgensen, F., & Sandersen, P. B. E. (2006). Buried and open tunnel valleys in Denmark—erosion beneath multiple ice sheets. *Quaternary Science Reviews*, *25*(11–12), 1339–1363. https://doi.org/10.1016/j.quascirev.2005.11.006

Kaufmann, F. J. (1872). *Gebiete der Kantone Bern, Luzern, Schwyz und Zug*. J. Dalp. Bern, 534 pp.

Kehew, A. E., Piotrowski, J. A., & Jørgensen, F. (2012). Tunnel valleys: Concepts and controversies—a review. *Earth-Science Reviews*, *113*(1-2), 33–58. https://doi.org/10.1016/j.earscirev.2012.02.002

Kemp, E. M. (1976). *Palynological observations in the Officer Basin, Western Australia*. Australia Bureau of Mineral Resources, Geology and Geophysics, Record, 160.

Kennewell, P. J. (1977). *Explanatory notes on the Yowalga 1:250 000 geological sheet, Western Australia SG/51-12*. 1:250 000 Geological Series, Explanatory Notes, 17.

Kessler, T. C., Klint, K. E. S., Nilsson, B., & Bjerg, P. L. (2012). Characterization of sand lenses embedded in tills. *Quaternary Science Reviews*, *53*, 55–71. https://doi.org/10.1016/j.quascirev.2012.08.011

Kjær, K. H., Sultan, L., Krüger, J., & Schomacker, A. (2004). Architecture and sedimentation of outwash fans in front of the Mýrdalsjökull ice cap, Iceland. *Sedimentary Geology*, *172*(1-2), 139–163. https://doi.org/10.1016/j.sedgeo.2004.08.002

Krüger, J. (1984). Clasts with stoss-lee form in lodgement tills: A discussion. *Journal of Glaciology*, *30*(105), 241–243. https://doi.org/10.3189/S0022143000006006

Krüger, J. (1994). Glacial processes, sediments, landforms, and stratigraphy in the terminus region of Myrdalsjökull, Iceland: Two interdisciplinary case studies. *Folia Geographica Danica*, *21*, 233 p.

Laws, J. (1980). *Report on Groundwater Prospects– Cundeelee Mission*. Geological Survey Western Australia. Hydrogeology Report 2201.

Le Heron, D. P., Heninger, M., Baal, C., & Bestmann, M. (2020). Sediment deformation and production beneath soft-bedded Palaeozoic ice sheets. *Sedimentary Geology*, *408*, 105761. https://doi.org/10.1016/j.sedgeo.2020.105761

Lipka, E. (2025). Morphological insights into tunnel valley formation and associated landforms: A case study from western Poland. *Landform Analysis*, *43*, 69–79. https://doi.org/10.12657/landfana-043-006

Lister, H. (1981). Particle size, shape, and load in a cold and a temperate Valley Glacier. *Annals of Glaciology*, *2*, 39–44. https://doi.org/10.3189/172756481794352397

Livingstone, S. J., & Clark, C. D. (2016). Morphological properties of tunnel valleys of the southern sector of the Laurentide Ice Sheet and implications for their formation. *Earth Surface Dynamics*, *4*(3), 567–589. https://doi.org/10.5194/esurf-4-567-2016

Lukas, S., Benn, D. I., Boston, C. M., Brook, M., Coray, S., Evans, D. J. A., Graf, A., Kellerer-Pirklbauer, A., Kirkbride, M. P., Krabbendam, M., Lovell, H., Machiedo, M., Mills, S. C., Nye, K., Reinardy, T. I., Ross, F. H., & Signer, M. (2013). Clast shape analysis and clast transport paths in glacial environments: A critical review of methods and the role of lithology. *Earth-Science Reviews*, *121*, 96–116. https://doi.org/10.1016/j.earscirev.2013.02.005

Lynham, L. (2021). *A fresh Look at the Stratigraphy of the Lefroy Palaeodrainage System*, Eastern Goldfields, WA. ARGA Symposium, Australian Earth Sciences Convention 9–12th February 2021.

Magee, J. W. (2009). Palaeovalley groundwater resources in arid and semi-arid Australia– a literature review. *Geoscience Australia Record*, *2009/03*, 224 p.

Magrani, F., Valla, P. G., Gribenski, N., & Serra, E. (2020). Glacial overdeepenings in the Swiss Alps and foreland: Spatial distribution and morphometrics. *Quaternary Science Reviews*, *243*, 106483. https://doi.org/10.1016/j.quascirev.2020.106483

Mamuse, A., & Guj, P. (2011). Rank statistical analysis of nickel sulphide resources of the Norseman-Wiluna Greenstone Belt, Western Australia. *Mineralium Deposita*, *46*(3), 305–318. https://doi.org/10.1007/s00126-011-0333-z

Matthews, J. A. (1987). Regional variation in the composition of Neoglacial end moraines, Jotunheimen, Norway: An altitudinal gradient in clast roundness and its possible palaeoclimatic significance. *Boreas*, *16*(2), 173–188. https://doi.org/10.1111/j.1502-3885.1987.tb00769.x

Menzies, J. (2023). Glacial microsedimentology—a new lens to investigate glacial sediments—a review. *Canadian Journal of Earth Sciences*, *60*(4), 366–387. https://doi.org/10.1139/cjes-2022-0048

Menzies, J., Gao, C., & Kodors, C. (2013). Microstructural analyses of a Middle Pliocene till from the James Bay Lowlands, Canada—evidence of "potential" fast ice streaming. *Proceedings of the Geologists' Association*, *124*(5), 790–801. https://doi.org/10.1016/j.pgeola.2012.07.002

Menzies, J., & Meer, J. J. M. (2018). Micromorphology and Microsedimentology of Glacial Sediments. In J. Menzies & J. J. M. van der Meer (Eds.), *Past glacial environments* (2nd ed., pp. 753–806). Elsevier Ltd. https://doi.org/10.1016/b978-0-08-100524-8.00036-1

Menzies, J., van der Meer, J. J. M., & Ravier, E. (2016). A kinematic unifying theory of microstructures in subglacial tills. *Sedimentary Geology*, *344*, 57–70. https://doi.org/10.1016/j.sedgeo.2016.03.024

Miall, A. D. (1996). *The geology of fluvial deposits: Sedimentary facies, basin analysis, and petroleum geology*. Springer.

Molén, M. O. (2023). Glaciation-induced features or sediment gravity flows—An analytic review. *Journal of Palaeogeography*, *12*(4), 487–545. https://doi.org/10.1016/j.jop.2023.08.002

Montgomery, D. R. (2002). Valley formation by fluvial and glacial erosion. *Geology*, *30*(11), 1047–1050. https://doi.org/10.1130/0091-7613(2002)030<1047:VFBFAG>2.0.CO;2

Morgan, K. H. (1993). Development, sedimentation and economic-potential of palaeoriver systems of the Yilgarn Craton of Western-Australia. *Sedimentary Geology*, *85*(1-4), 637–656. https://doi.org/10.1016/0037-0738(93)90106-F

Mory, A. J., Redfern, J., & Martin, J. R. (2008). A review of Permian–Carboniferous glacial deposits in Western Australia. In C. R. Fielding, T. D. Frank, & J. L. Isbell (Eds.). *Late Devonian and Early Carboniferous glacial records of South America* (pp. 29–40). Geological Society of America Special Paper 441. https://doi.org/10.1130/2008.2441(02)

Normington, V. J., Hill, S. M., Tiddy, C. J., & Giles, D. (2018). *Sedimentology of the late Palaeozoic Cape Jervis Formation, Troubridge Basin, South Australia*. Government of South Australia, Departmental Publication - Geological Survey Geoscience. Report Book 2018/00026. https://pid.sarig.sa.gov.au/document/2018d051417

Oxenburgh, S., Falconer, M., Doutch, D., Edmonds, P., Foley, A., & Jane, M. (2017). Kambalda—St Ives goldfield. In G. N. Philips (Ed.), *Monograph 32—Australian ore deposits* (pp. 215–222). The Australasian Institute of Mining and Metallurgy.

Patton, H., Swift, D. A., Clark, C. D., Livingstone, S. J., & Cook, S. J. (2016). Distribution and characteristics of overdeepenings beneath the Greenland and Antarctic ice sheets: Implications for overdeepening origin and evolution. *Quaternary Science Reviews*, *148*, 128–145. https://doi.org/10.1016/j.quascirev.2016.07.012

Paul, M. A., & Eyles, N. (1990). Constraints on the preservation of diamict facies (melt-out tills) at the margins of stagnant glaciers. *Quaternary Science Reviews*, *9*(1), 51–69. https://doi.org/10.1016/0277-3791(90)90004-T

Pérez Loinaze, V. S., Limarino, C. O., & Césari, S. N. (2011). Glacial events in Carboniferous sequences from Paganzo and Río Blanco basins (northwest Argentina): Palynology and depositional setting. *Geologica Acta*, *8*(4), 399–418. https://doi.org/10.1344/105.000001579

Pickard, A. (2025). *Karonie; For the Period 24 April 2017 to 22 April 2025. Karonie Project E28/2642*. *Final Surrender Report*. Alchemy Resources.

Playford, P. E. (2001). *The Permian–Carboniferous glaciation of Gondwana: Its legacy in Western Australia*. Geological Survey of Western Australia. Record, 2001/5.

Prasicek, G., Otto, J-C., Montgomery, D. R., & Schrott, L. (2014). Multi-scale curvature for automated identification of glaciated mountain landscapes. *Geomorphology (Amsterdam, Netherlands)*, *209*(100), 53–65. https://doi.org/10.1016/j.geomorph.2013.11.026

Rampe, E. B., Horgan, B. H. N., Smith, R. J., Scudder, N. A., Bamber, E. R., Rutledge, A. M., & Christoffersen, R. (2022). A mineralogical study of glacial flour from Three Sisters, Oregon: An analog for a cold and icy early Mars. *Earth and Planetary Science Letters*, *584*, 117471. https://doi.org/10.1016/j.epsl.2022.117471

Rust, B. R. (1975). Fabric and structure in glaciofluvial gravels. In A. V. Jopling & B. C. McDonald (Eds.), *Glaciofluvial and Glaciolacustrine sedimentation* (Vol. 23, pp. 238–248). SEPM Society for Sedimentary Geology. https://doi.org/10.2110/pec.75.23.0238

Salama, W., & Anand, R. R. (2017). Reconstructing the pre-Quaternary landscape in Agnew–Lawlers area, Western Australia with emphasis on the Permo-Carboniferous glaciation and post-glacial weathering. *International Journal of Earth Sciences*, *106*(1), 311–339. https://doi.org/10.1007/s00531-016-1320-5

Salama, W., Anand, R. R., Tunmer, W., & Aspandiar, M. (2022). Regolith characterization and landscape evolution for geochemical exploration of the covered Yamarna Terrane, Western Australia. *Journal of Geochemical Exploration*, *232*, 106881. https://doi.org/10.1016/j.gexplo.2021.106881

Salama, W., Verrall, M., Culver, K., & Anand, R. R. (2021). Interface sampling and indicator minerals for detecting the footprint of the Lancefield North gold deposit under the Permian glacial cover in Western Australia. *Minerals*, *11*(10), 1131. https://doi.org/10.3390/min11101131

Scotese, R. C., & Barrett, S. F. (1990). Gondwana's movement over the South Pole during the Palaeozoic: Evidence from lithological indicators of climate. In W. S. McKerrow & C. R. Scotese (Eds.), *Palaeozoic Palaeogeography and Biogeography* (pp.75–85). Geological Society. 12. https://doi.org/10.1144/GSL.MEM.1990.012.01.06

Sharp, M. (1982). Modification of clasts in lodgement tills by glacial erosion. *Journal of Glaciology*, *28*(100), 475–481. https://doi.org/10.3189/S0022143000005062

Siman-Tov, S., Stock, G. M., Brodsky, E. E., & White, J. C. (2017). The coating layer of glacial polish. *Geology*, *45*(11), 987–990. https://doi.org/10.1130/G39281.1

Sissons, J. B. (1961). A subglacial drainage system by the Tinto Hills, Lanarkshire. *Transactions of the Edinburgh Geological Society*, *18*(2), 175–193. https://doi.org/10.1144/transed.18.2.175

Sneed, E. D., & Folk, R. L. (1958). Pebbles in the Lower-Colorado-River, Texas a Study in Particle Morphogenesis. *The Journal of Geology*, *66*(2), 114–150. &. https://doi.org/10.1086/626490

Sofoulis, J. (1965). Explanatory notes on the Widgiemooltha 1:250 000 geological sheet, Western Australia. *Geological Survey of Western Australia*, *1965/10*, 41 p.

Sofoulis, J., & Bock, W. (1962). *Progress report on the regional survey of the Widgiemooltha sheet area SH54-14, international series*. Geological Survey of Western Australia.

Stewart, M., Lonergan, L., & Hampson, G. (2012). 3D seismic analysis of buried tunnel valleys in the Central North Sea: Tunnel valley fill sedimentary architecture. In M. Huuse, J. Redfern, D. P. Le Heron, R. J. Dixon, A. Moscariello & J. Craig (Eds.), *Glaciogenic Reservoirs and Hydrocarbon Systems.* (pp.173–184) Geological Society. Special Publication 368. https://doi.org/10.1144/SP368.9

Stewart, M., Lonergan, L., & Hampson, G. (2013). 3D seismic analysis of buried tunnel valleys in the central North Sea: Morphology, cross-cutting generations and glacial history. *Quaternary Science Reviews*, *72*, 1–17. https://doi.org/10.1016/j.quascirev.2013.03.016

Talbot, H. W. B. (1920). The geology and mineral resources of the Northwest, Northeast and Central Divisions. *Geological Survey of Western Australia Bulletin*, (*83*), 205.

Tapley, I. J. (1988). The reconstruction of palaeodrainage and regional geologic structures in Australia's canning and officer basins using NOAA-AVHRR satellite imagery. *Earth-Science Reviews*, *25*(5-6), 409–425. https://doi.org/10.1016/0012-8252(88)90008-6

Tedesco, J., Cagliari, J., Coitinho, J. d R., Lopes, R. d C., & Lavina, E. L. C. (2016). Late Paleozoic paleofjord in the southernmost Parana Basin (Brazil): Geomorphology and sedimentary fill. *Geomorphology*, *269*, 203–214. https://doi.org/10.1016/j.geomorph.2016.06.035

Traves, D. M., Wells, A. T., & Casey, J. N. (1956). *The geology of the south-western Canning Basin, Western Australia*. Bureau of Mineral Resources, Geology and Geophysics.

Ugelvig, S. V., Egholm, D. L., Anderson, R. S., & Iverson, N. R. (2018). Glacial erosion driven by variations in meltwater drainage. *Journal of Geophysical Research: Earth Surface*, *123*(11), 2863–2877. https://doi.org/10.1029/2018JF004680

Van de Graaf, W. J. E., Crowe, R. A., Bunting, J., & Jackson, M. J. (1977). Relict early Cainozoic drainages in arid Western Australia. *Zeitschrift Fur Geomorphologiey*, *21*, 379–400. https://doi.org/10.1127/zfg/21/1977/379

Veevers, J. J. (1994). Case for the Gamburtsev subglacial mountains of East Antarctica originating by mid-Carboniferous shortening of an intracratonic basin. *Geology*, *22*(7), 593–596. https://doi.org/10.1130/0091-7613(1994)022<0593:CFTGSM>2.3.CO;2

Veevers, J. J. (2006). Updated Gondwana (Permian–Cretaceous) earth history of Australia. *Gondwana Research*, *9*(3), 231–260. https://doi.org/10.1016/j.gr.2005.11.005

Vielreicher, N., Groves, D., McNaughton, N., & Fletcher, I. (2015). The timing of gold mineralization across the eastern Yilgarn craton using U–Pb geochronology of hydrothermal phosphate minerals. *Mineralium Deposita*, *50*(4), 391–428. https://doi.org/10.1007/s00126-015-0589-9

Vives, C. R., Bendtsen, J., Dahms, R. D., Daugbjerg, N., Larsen, K. V., & Rosing, M. T. (2025). Trace metal distributions in the transition zone from the Greenland Ice-Sheet to the surface water in Kangerlussuaq fjord (67°N). *EGU. The Cryosphere*, *19*(8), 3107–3121. https://doi.org/10.5194/tc-19-3107-2025

Westaway, J. M., & Wyche, S. (1998). *Geology of the Darlot 1: 100 000 sheet*. Western Australia Geological Survey 1: 100 000 Geological Series Explanatory Notes.

White, W. A. (1972). Deep erosion by continental ice sheets. *Geological Society of America Bulletin*, *83*(4), 1037–1056. https://doi.org/10.1130/0016-7606(1972)83[1037:Debcis]2.0.Co;2

Ziegler, A. M., Hulver, J. M., & Rowley, D. B. (1997). Permian world topography and climate. In I. P. Martini (Ed.), *Late glacial and postglacial environmental changes: Quaternary, Carboniferous–Permian, and Proterozoic* (pp. 111–146). Oxford University Press.